Mechanical and Micro Structural Analysis of Dissimilar Weld Joints

A dissertation submitted in partial fulfilment of requirement for the award of degree of

Master of Engineering

in

Production Engineering

Submitted by

SHIVANI JHA

801585023

Under the guidance of

Dr. Ajay Batish
Professor

Dr. Deepa Mudgal
Assistant Professor

DEPARTMENT OF MECHANICAL ENGINEERING

THAPAR UNIVERSITY

PATIALA (PB), INDIA, 147004

July, 2017

Certificate

I hereby declare that the work done in this dissertation entitled "**Mechanical and Micro Structural Analysis of Dissimilar Weld Joints**" submitted towards partial fulfillment of requirement for award of degree of **Master of Engineering** in **Production Engineering, Thapar University, Patiala,** is an authentic record of the work carried out by me under the supervision and guidance of **Dr. Ajay Batish, Professor, Mechanical Engineering Department, Thapar University, Patiala** and **Dr. Deepa Mudgal, Assistant Professor, Mechanical Engineering Department, Thapar University.**

The matter embodied in this report has not been submitted in part or full to any other university or institute for the award of any degree.

Shivani

Dated: 18-08-2017

SHIVANI JHA

801585023

This is to certify that above declaration made by the student concerned is correct to the best of our knowledge and belief.

.....

Dr. Ajay Batish

Professor

Mechanical Engineering Department

Thapar University, Patiala

Deepa

.....

Dr. Deepa Mudgal

Assistant Professor

Mechanical Engineering Department

Thapar University, Patiala

Dedicated to

My loving parents…

Acknowledgements

I would like to express my deepest sense of gratitude and a very sincere thanks to my guide **Dr.Ajay Batish**, Professor, Mechanical Engineering Department, Thapar University, Patiala and **Dr. Deepa Mudgal**, Assistant Professor, Mechanical Engineering Department, Thapar University, Patiala for their sincere and invaluable guidance and full support which helped me in the accomplishment of this thesis report in present form. His dynamic and diligent enthusiasm has been highly instrumental in keeping my spirits high. His flawless and forthright suggestions blended with an innate intelligent application have crowned my task with success.

I am also thankful to **Dr. S. K. Mohapatra,** Head of Department, Mechanical Engineering and **Dr. Vinod Kumar Singla**, P.G coordinator, Production Engineering for providing us with the adequate infrastructure in carrying out the work.

I would like to thank the entire faculty and staff of Mechanical Engineering Department specially Mr. Mohinder Suri, Lab Instructor, Mechanical Department and my friends who devoted their valuable time and help me in all possible ways towards successful completion of this work. I thanks all those who have contributed directly or indirectly to this work.

Lastly, I would like to thank my family for their years of guidance, support, and encouragement. It would not have been possible without them to reach upto this point. They have always wanted the best for me and I admire their determination and sacrifices.

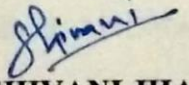

SHIVANI JHA

801585023

ABSTRACT

In power generation industries, there is a wide application of joining low alloy metals to austenitic stainless steel which are known as dissimilar weldments. These dissimilar metal joint have their applications in nuclear power plants and aerospace industries due to high strength at both high and room temperature conditions. A metal joint of low alloy steel and austenitic stainless steel provides a good blend of mechanical properties, weldability and formability. The demand of dissimilar welding arises due to better performance and economic benefits. As this technique involves the metal joints whose melting points, coefficient of thermal expansion and chemical compositions are unlike. It was very well known that, severe gradients in thermal and mechanical loading were exist in boilers used in power plant industries. The parts of boiler that are headed under the low temperature zone can be made with low alloy steel and rest part is to be constructed by austenitic steel for economic reason. Those dissimilar joints having austenitic steels have very prone to unexpected phase propagation which results in major mechanical and metallurgical changes. Therefore, it is very necessary to optimize the parameters such as (arc length, current, gas flow rate, type of fillers and types of grooves) so as to develop sound weld. Hence in the present study two dissimilar metals are welded that is SS316 and SS410 using TIG welding technique. In the experiment, L18 orthogonal array is applied by varying welding parameters. Micro hardness, tensile strength, optical microscopy and scanning electron microscopy was performed on the 18 trials obtained from orthogonal array. From the fractography, mostly the ductile fracture occur from AISI 410 side and some fracture has been occurring at the mid or weld joint. The significant factors affecting the micro hardness are current, arc length and type of fillers. The micro hardness increases with the decrease in current. From the microstructures the grain coarsening, segregations, skeleton structure and vermicular structures were observed in the weld bead.

Keywords: GTAW; Dissimilar Weld Joints; FESEM; SS410: SS316; Taguchi Method; ANOVA

TABLE OF CONTENTS

LIST OF FIGURES

LIST OF TABLES

CHAPTER-1

INTRODUCTION

1.1 WELDING

Welding is termed as metal joining process and finds its basic existence in manufacturing sector. Welding is a process of fabrication between two or more parts by the application of heating upto the melting temperature to make a joint of high strength.by the application of filler or pressure if required. The filler and base metal have their melting point nearly same. "[1]. It is also known as a positive process and for permanent joint.

1.2 SIGNIFICANCE OF WELDING

There is a gradually increasing in demand of more precise specimens and high production rates, fully automated and the welding processes that are mechanized have taken a pre-eminent occurrence in the field of welding area. It means the pace at which the automated machines are introduced in the welding field for various welding process is unremarkable. Moreover, computers are contributing an essential role in the automated welding programs which needs algorithms including various mathematical equation and welding parameters so as to make the welding process done accurately.

1.3 CATEGORIZATION OF WELDING PROCESS

There are basically two types of welding processes which are categorized as

(a) Fusion Welding or Non Pressure Welding

(b) Plastic Welding or Pressure Welding

(a) Fusion Welding or Non Pressure Welding: It is a fusion process of joining the base metal to make the weld. The heat, shielding and filler material are the essential requirement of joining the fusion process.

(b) Plastic Welding or Pressure Welding: It is a process in which the metal is heated to a plastic state which is subjected to the external pressure force to form a joint. The most important factor in this welding process is the externally applied force to make the weld. It is a process in which the coalescence is produced below the melting point temperature of the

base metal which is being joined without filler material addition. The uniqueness of this process is that the metal is not melted and the mechanical properties are not affected. It is also known as a solid state welding process.

1.4 TYPES OF FUSION WELDING PROCESS

Fusion Welding process are categories as

Table1.1: General Characteristics Of fusion welding process [2]

Joining Process	Operation	Advantage	Skill Level Required	Welding position	Current type	Distortion	Cost of Equipment
Shielded metal-arc	Manual	Portable and flexible	High	All	AC, DC	1or 2	Low
Submerged	Automatic deposition	High medium	Low to high	Flat and horizontal	AC, DC	1 to 2	Medium
Gas-metal arc	Semi-automatic or automatic	Most metals	Low to high	All	DC	2 to 3	Medium to high
Gas tungsten-arc	Manual or automatic	Most metals	Low to high	All	AC, DC	2 to 3	Medium
Flux-cored arc	Semi-automatic or automatic	High deposition	Low to high	All	DC	1 to 3	Medium
Oxy-fuel	Manual	Portable and Flexible	High	All	_	_	Low

Electron-beam, Laser-Beam	Semi-automatic or automatic	Most metals	Medium to high	All	_	3 to 5	High

1.5 GAS TUNGSTEN ARC WELDING

1.5.1 Process

The GTAW (Gas Tungsten Arc Welding) or TIG is employed where the high quality weld and good weld appearance is required. In TIG, the applied heat melts and join the metal with an established arc between the metal and non consumable tungsten electrode. The torch which holds the tungsten electrode is in contact with the shielding gas cylinder and the power source. The is water cooled tube made up of copper which are in contact with tungsten electrode which is in contact with the terminal by the welding cable (cable 1). Due to this, the welding current entered into the electrode from the power source and the electrode overheating is prevented by water cooled jackets. With the help of cable 2, the work piece is connected to the second terminal of the power source. The shielding gas is passed by the torch and is directed by the nozzle to protect the weld pool from air. Mainly, inert gases i.e. argon and helium are used as shielding gases. For joining thicker materials, filler rod needs to be fed either automatically or manually into the arc [3].

1.5.2 Polarity

There are three polarities which are used i.e. DCEP, DCEN and AC

(a) DIRECT CURRENT ELECTRODE NEGATIVE (DCEN): DCEN is the most commonly used polarity in GTAW and also known as straight polarity. The negative terminal of the electrode is connected to the power supply. A significant amount of energy is provided by the source to develop work function so the electrons are emitted and accelerated from the tungsten electrode through the arc to the workpiece [3]. DCEN results into a narrow and deep weld [4].

(b) DIRECT ELECTRODE CURRENT POSITIVE (DCEP): DCEP is also known as reverse polarity. In this case, the positive terminal is coupled with the electrode of the power source. The heat affect caused by the electrode is not on the work piece but will be on the tungsten electrode. Water cooled electrodes are utilized for large diameters in order to avoid

electrode tip melting. A shallow and clean weld is obtained. For welding thin sheets like aluminum and magnesium, DCEP is utilized [3].

(c) ALTERNATING CURRENT (AC): A.C. is mainly used for welding aluminum alloys. Good oxide cleaning action and penetration is achieved [3].

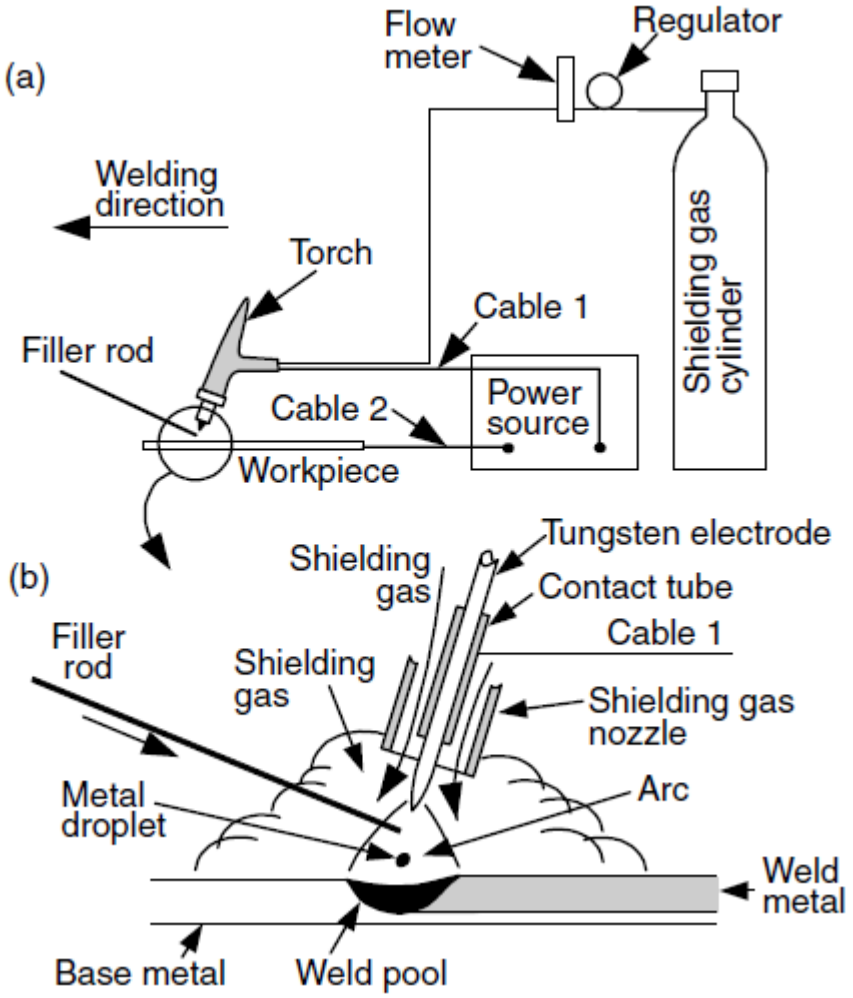

Fig1.1: The gas tungsten arc welding (a) process (b) welding area enlarged [3]

1.5.3 Electrodes

Tungsten electrode containing 2% of thorium or cerium possess better current-carrying capacity, electron emissivity and resistance to contamination on the contrary with pure tungsten electrodes. Arc initiation is easier and more stable. The emitting ability of electron tip to emit electrons is known as electron emissivity. When higher electrode temperature resulting into emitted electrons signifies lower electron emissivity and resulting into a greater risk of electrode tip melting [3].

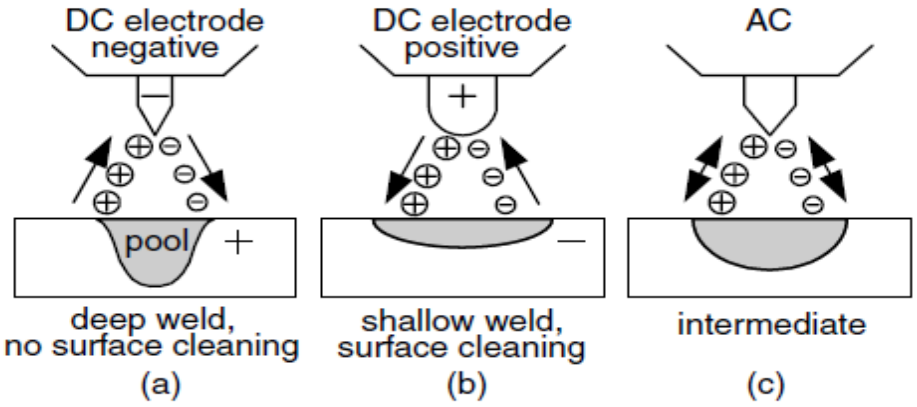

Fig1.2 Three different polarities in GTAW [3]

1.5.4 Shielding gas

Mostly argon and helium are utilized as shielding gas. Argon is ionized more easily than helium as arc initiation is quiet easier along with lower voltage drop. As the weight of argon is more than helium, it offers more resistance to cross draft. Moreover it also gives more effective shielding effect than helium. Argon has more oxidizing cleaning action than helium while applying DCEP or AC. The good effects which are mention above and the lower cost of argon than helium make argon more attractive [3].

1.6 EFFECT OF WELDING PARAMETERS ON GTAW

The parameters that affect the outcome and quality of the GTAW process are given below

(a) WELDING CURRENT: Lower in current subjected to sticking of the filler wire and higher in current leads to splatter that cause damage to the work piece [4, 5]. Larger heat affected area can be resulted into lower welding current. Sometimes at very low current, a larger heat affected area is observed as the deposition of same quantity of filler material takes larger time. To achieve constant arc current, the voltage can be varied by fixed current mode.

(b) WELDING SPEED: It is also the prominent factor in GTAW. Increasing in the welding speed results into the decrement into the heat input per unit length or power of the weld which also causes reduction in the penetration of weld and weld reinforcement. Weld bead size and penetration generally dominant on the welding speed and current also. Defects arises due to very high welding speed results into porosity, tendency of having undercut, uneven bead size and last but not the least decreases wetting action. Porosity can only be reduced at low welding speed.

(c) WELDING VOLTAGE: As per the GTAW equipment requirement, welding voltage can be adjustable or sometimes fixed. Large variability can be seen, when subjected to high welding voltage. A good extent of large working tip distance and easy arc initiation is associated with high arc initiation.

(d) INERT GAS: The factors which affects the selection of shielding gas are working metals, electrode, welding speed, splatter, weld temperature, cost etc. The reasons which is behind choosing the shielding gas are brittleness, corrosion resistance, hardness, strength, porosity, penetration depth and finished surface profile. Argon and helium are the most widely and successfully used for GTAW. For very thin welding, argon gas is recommended which results into good smooth arc. Arc penetration is reduced when argon is utilized that's why preferred in many applications than helium.

Table1.2: Various shielding gases can be used in GTAW process [3]

Gas	Chemical Symbol	Molecular Weight (g/mol)	Specific Gravity with Respect to Air at 1 atm and 0°C	Density (g/L)	Ionization Potential (eV)
Argon	Ar	39.95	1.38	1.784	15.7
Carbon dioxide	CO_2	44.01	1.53	1.978	14.4
Helium	He	4.00	0.1368	0.178	24.5
Hydrogen	H_2	2.016	0.0695	0.090	13.5
Nitrogen	N_2	28.01	0.967	1.25	14.5
Oxygen	O_2	32.00	1.105	1.43	13.2

1.7 ADVANTAGES AND DISADVANTAGES OF GTAW

1.7.1 Advantages of GTAW

The various benefits of GTAW are

1. No fumes and spatter in welding.
2. It can weld ferrous and non-ferrous metals.
3. Narrow concentrated arc.
4. No slag, spatter, smoky or sparks formation.
5. Does not use flux as shielding gas are employed to eliminate environmental contamination.
6. It is a very clean action process and high quality weld is achieved.

1.7.2 Disadvantages of GTAW

1. Higher level of UV rays.

2. It has low deposition rates.
3. It requires skilled operator.
4. It requires hand and eye coordination to acquire weld penetration.

1.8 LIMITATION OF GTAW

1. Restricted to horizontal and flat surfaces.

1.9 APPLICATIONS OF GTAW

1. Aircraft
2. Food processing industry
3. Automobile industry
4. Precision manufacturing industry
5. Maintenance repair wok
6. Nuclear industry

1.10 WELDING MATERIAL

Austenitic SS316 and martensitic SS410 stainless steel are selected for examination. Further introduction about the material will be given below in the sub sections.

1.10.1 Stainless steel

When there is some amount of carbon alloyed with iron, the steel is formed. Iron is crystalline in nature which exists in minimum two forms dependent on temperatures. The body centered cubic structure is the most stable face at high and low temperatures and moreover these also termed as α and δ delta ferrite respectively.

Stainless steel contains minimum 10.5% chromium and 7% of nickel which makes it corrosion resistant [5]. Stainless steel can be classified into three categories austenitic, martenstic and ferritic steel on the basis of the structure.

1.10.2 Austenitic Stainless Steel

Austenitic stainless steel has wide application in the containers, house wares, architectural facades, constructural structures, industrial pipings and industrial vessels due to its weldability and corrosion resistant features as they are having a very high ultimate tensile strength and low yeild strength that is why it is often ductile in nature [7]. Moreover, they are having very fine properties at cryogenic temperatures. Furthermore, these steels generally

contain 7-20% Ni, 16-25% Cr and less than 0.08% C. On adding, 2-6% Mo, 0.1-0.2% N and titanium or niobium in stabilized varieties can result into better corrosion resistant properties.

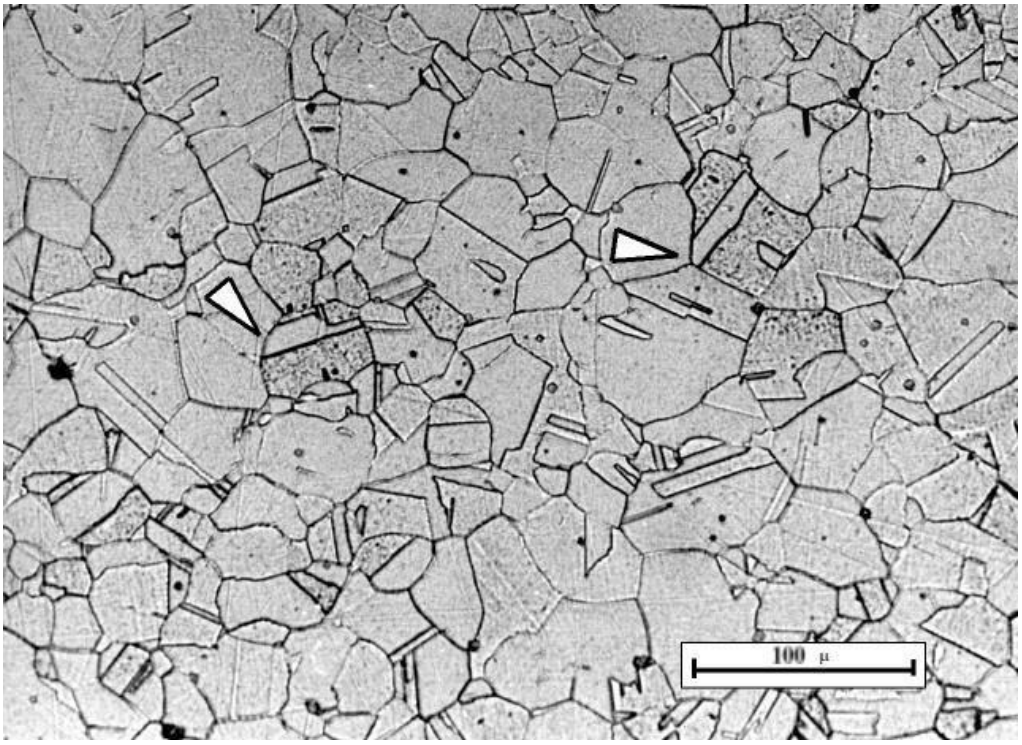

Figure 1.3 Grain structure of austenitic stainless steel [6]

As SS316 is also known as austenitic nickel chromium stainless steel. With the addition of molybdenum, the corrosion properties become better. In medical implants, the use of SS316 is growing as in stents and orthopedic replacement due to reasonable chemical stability, relatively low cost and ease of fabrication [8]. In comparison with SS304, it gives better crevice corrosion and pitting resistant property in chloride environment. In addition, it provides excellent welding and forming characteristics. Also in thin sections, post weld annealing is not required [9].

1.10.3 Martenistic stainless steel

Martanistic stainless steel is generally high or low carbon steels built around type 410 composition. It has orthorhombic microstructure observed in 1980 by Adolf Martens who was a German microscopist [8]. Martenistic stainless steel are widely employed in fabricating components for high resistance to wear, high strength and in industrial sectors and applications like oil extraction and drilling, thermoelectric plant, mining machinery and steam turbine [10].

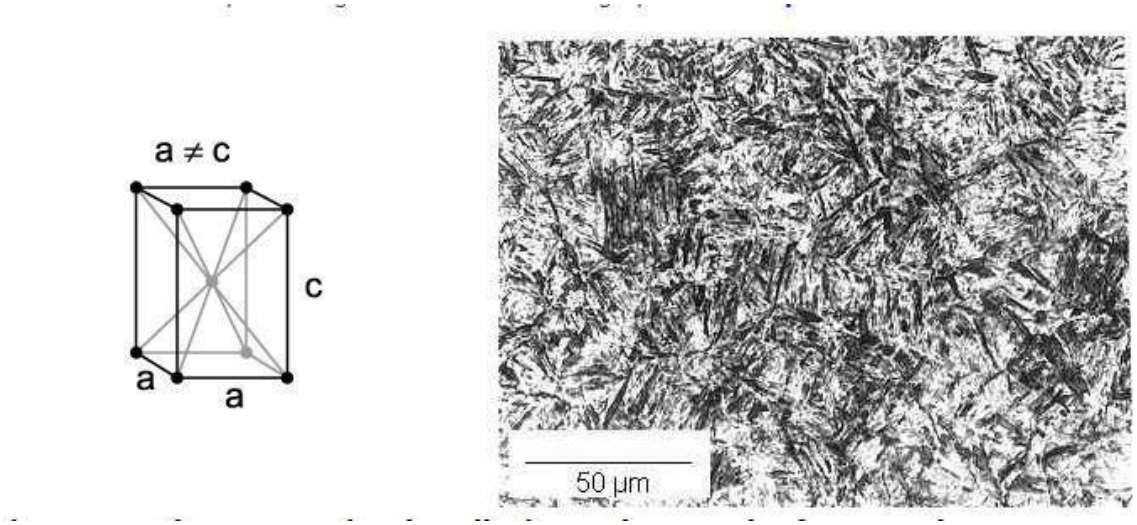

Figure 1.4: Body centered tetragonal unit cell matensite structure [11]

1.11 DISSIMILAR WELDING

Dissimilar welding is defined as the joining of two same metal by the use of heterogeneous filler or by using two different metal joints using the same or different metals. Now a days, dissimilar welding has a great role in this revolutionary world.

1.12 NEED OF WELDED DISSIMILAR METAL JOINTS

The main purpose of using dissimilar metal joints to reduce cost and makes it economical. Now a days, cost becomes a prominent factor with optimum quality. In power plant components, dissimilar metal joints needed due to severe gradients in thermal and mechanical loading. Moreover, the parts of boiler that are headed under the low temperature zone can be made with low alloy steel for economic reason. Rest part is to be constructed by austenitic steel [12]. Furthermore, it makes the efficient use of material which gives the flexible design to products and components.

1.13 WELDING DEFECTS

Defects can also leads to mechanical properties failure. Generally, the defects is basically a deviation from the required properties or it sometimes due to the lacking of operator skills and machine errors. As per the Indian Institute of Welding, the defects are categorizes into six areas i.e. Cracks, cavity defects, incomplete fusion, solid inclusion, imperfect shape and miscellaneous defects [13].

1.13.1 Cracks

The most dominant type of defect is crack as it reduces the efficiency of welded joint and can leads to catastrophic failure. There are various types of cracks resulted due to longitudinal crack, crater cracks, transverse cracks, toe cracks and under bead cracks. These above mentioned defects are visible too and named as surface defects. The reason behind the crack is generally high concentration stress that is due to poor-fit up, solidification of weld, poor edge quality and incorrect welding procedure. By reducing the cooling rate, pre heating the joint and taking important consideration during post weld heat treatments are some of the remedies for avoiding the cracks [13].

1.13.2 Shrinkage Cavities

These cavities are formed by the solidification of weld metal which leads to shrinkage. To avoid this defect, there should be a proper amount of filler material is filled [13].

1.13.3 Blowholes and porosities

These are the defects that are generally seen at the sub surfaces in the weld joint such as actually voids, cavities or holes that is formed by the entrapped gases Porosity not considered as serious a defect as cracks since the porosity cavities usually have rounded ends which are not expected to propagate as cracks in the weldments [13].

1.13.4 Slag inclusions

It is a type of defect that includes the phosphorus compounds, nitrides and solidified flux that comprises of oxides which are not able to float out to the surface and will entrapped in the weld joint. At high current and DCEP GTAW welding, inclusions of tungsten electrode occurs. Such inclusions results into intermittent, continuous and randomly placed. These defects reduces the ductility of the welds mainly [13].

1.13.5 Incomplete penetration and fusion

Due to the offset of electrode from weld axis, inadequate welding current, increasing welding speed, fit -up and improper joint preparation can leads to incomplete fusion. Its generally arises between weld metal and parent metal and in between the intermediate layers of multi pass welding [13].

1.13.6 Imperfect Shape

Overlap, Excessive reinforcement, under fill, under cut, dimensional deviations, bead shape, and excessive penetration are the types of imperfect shape. Suck bars and under fills usually occurs due to uneven depression (such as concave contour) respectively on the root or face surface of the weld that is extending below the surface of the adjacent base metal. Both of

the two decreases the cross sectional area of weld joint as per the designated specifications. At that point failure occurs due to stress raiser and weak point.

Due to the poor fit, improper welding technique, too wide root gap or too small a root face, excessive welding current and poor fit-up leads to excessive penetration and excessive reinforcement that is undesirable in a weld joint [13].

.

Chapter 2
LITERATURE REVIEW

2.1 LITERATURE REVIEW

The very first step to analyze the research is the literature review. A wide range of literature can be extracted from journals and books on the austenitic steel grades i.e. SS316 and SS410. From the dissimilar metal joint of grade SS316 and SS410, the effect of welding properties and corrosion resistance properties can be explained.

Arivazhagan et al. (2011) investigated AISI 4140 low alloy steel and AISI 304 austenitic steel dissimilar joints by EBW (LOW KW), Continuous drive FRW (capacity 150 KN) and GTAW (DCEN). Microstructure, phase composition and mechanical properties are analyzed for each of the weldments. Three of them techniques produce sound weldments.

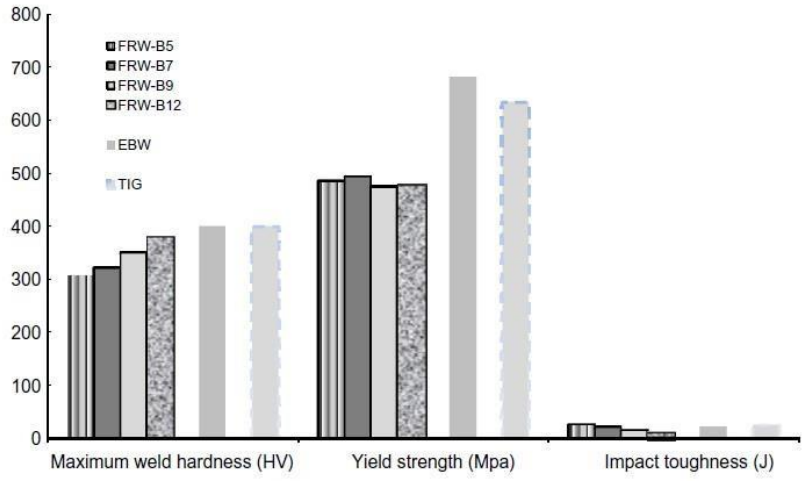

Figure 2.1: Bar charts indicating cumulative mechanical properties of dissimilar weldmets AISI 304 AND AISI 4140 by GTAW, FRW and EBW

From the tensile analysis, the EBW has the highest tensile strength (681MPa) relatively with GTAW (635MPa) and FRW (494MPa) as the failure for FRW occurs at the side of AISI 4140 and for GTAW and EBW, the failure in AISI 4140 is observed at HAZ. Higher impact strength is given by GTAW among the applied techniques [13].

Falat et al. (2012) examined the microstructural characteristics of T91/TP316 Haustenitic/martensitic dissimilar weldments constitutes Ni-based weld metal with GTAW. In this analysis, scanning electron microscopy, energy dispersive X-ray spectroscopy, Transmission electron microscopy and light microscopy were used. A wide heat effected zone showing typical micro structural gradient ranging from coarse grain structure to fine grain/ intercritical region in the part of martenistic welded joint. On the contrary, the austenitic steel HAZ was restricted to narrow region that contains the coarsened polygonal grains as a result of phase transformation from austenitic to martenistic steel during the welding [14].

Chen et al. (2013) examined the mechanical and micro structural properties of super 304H/T92 dissimilar weld joints succeeding with high temperature ageing is done with GTAW. In this, the dissimilar metal tubes of diameter 51 mm and thickness 11 mm is taken and filler ERNiCr-3 is chosen. After PWHT, the microstructures is seen and ageing is done with the help of X ray NDT at 650°C for certain hours(100h, 500h, 1000h and 3000h). As the ageing time is increased, in the HAZ of T92 side and the base metal, second -phase particles aggregate and coarsen in the austenitic grains. On the contrary, in HAZ and BM of Super 304H side, the growth of austenitic grains and that of second phase particles are less. The fracture position in he aged Super 304H/T92 joints is always seen in the T92 BM. With the increase in ageing time, the tensile strength of the weld joints drops sharply in the first stage, then it reaches to the maximum value and at the end it tends to be constant which is similar in the change in the hardness value in the HAZ of T92 side and BM of the weld joint against the age time [15].

Hosseini et al. (2016) discussed the weldability and micro structural of AISI 310/Inconel 617 dissimilar welds using DCEN GTAW. 12mm sheet of inconel 617 and SS310 is taken and three fillers (ERNiCr3, ERNiCrMo 1 and ER310) are chosen. Welding parameters are chosen as current 140 Amp voltage ranges from 17-20V welding speed 1.063-1.73mms^{-1}. Many distinct cracks in the weld joint is shown in ER 310 SS filler metal as per the micro structural observations. Inconel 617 shows the greatest influence which causes resistance to cracking because of solidification due to the amount of left liquid film and solidification temperature range. As the alloy melting range increases in the pesecnce of the phenomenon of cyclic thermal stress that favors the hot cracking in the HAZ of the weld joints employing ERNiCr3 and ER310 filler material [16].

Ramkumar et al. (2015) investigated the effect of filler addition on the tensile strength and microstructure of dissimilar weld joints of AISI 416 and Inconel 718 using Autogenous

tungsten inert gas welding. A 5mm hot rolled sheet of both Inconel 718 and AISI 416is employed and the flux used is pure TiO_2 that is added with methanol to get paint like consistency. Optical microscopy and SEM is used for the microstructure examination. In AISI 416, the fine martensite is present in HAZ and in Inconel 718, there is a presence of unmixed zone including HAZ at secondary phases. Lave phase and Nb rich eutectic were analyzed at the fusion zone of both weld joints. Joint tensile strength with flux addition is greater than with no flux and fracture is noticed at the fusion zone in both cases. Complete penetration due to high energy density in a single pass is achieved with flux and a total heat input is less compared to others with no flux [17].

Hajiannia (2013) studied the microstructure and mechanical properties of A355 low alloy steel and AISI 347 stainless steel dissimilar weld joint prepared by DCEN GTAW. The low alloy steel A335 and 347 austenitic steel of 8 mm thick, 400 mm long and 200 mm in outside diameter and two fillers (ER309L and ERNiCr-3) are employed with DCEN polarity and argon gas shield of 99.99%. All weld joints are unsuccessful in the HAZ A335 in tensile testing. All specimens are showing ductile fracture in the impact test results. ERNiCr-3 gives the optimum mechanical properties for the dissimilar weld joint of A335 low alloy steel and AISI 347 [18].

Cao et al. (2011) studied the microstructure and mechanical properties of dissimilar weld joints between S304H austenitic and T92 martensitic steels produced by GTAW. Impact toughness and tensile strength of S304H/T92 dissimilar weld joint meets the requirement of USC boiler. T92 coarsed grained HAZ part have relatively weak tensile strength due to coarsed tempered martensitic structure and the part which have relatively weak toughness is weld metal due to coarse dendritic austenitic structure. (19)

Ramkumar et al. (2012) analyzed the effect of filler material on the performance of dissimilar weld joint of AISI 304 and Monel 400 produced by GTAW. In this experiment, E309L and ENiCu-7 are employed. The specimen dimensions are 100*50*6 mm with a standard butt joint configuration. In this, K_2SO_4+NaCl (60%) molten salt environment and cyclic air oxidation at 600°C. The reason of hot corrosion in E309L weld joint is the micro segregation of Cu ad Cr in the weld interface at the dendrite structures in weld metal. ENiCu-7 filler shows better tensile strength than E309L.The ductility and strength of ENiCu-7 welds are comparable to those of Monel 400/ AISI 304. All the weld joints are showing an increasing corrosion rate when subjected to molten salt environment. No weight gain is seen in air oxidation environment. The

overall performance based on mechanical, metallurgical and corrosion resistance could be like this $W_{ENiCu-7}$ and W_{E309l}[20].

Ramkumar et al. (2015) investigated the mechanical and metallurgical characterization of dissimilar welds of super duplex stainless steel and austenitic stainless steel produced by GTAW. In this experiment, two fillers are used i.e ER2553 and ERNiCrMo-3.The specimen dimensions are 150 mm*55 mm*5 mm using CCGTA and PCGTA welding. Weld zone and interfacial microstructure were analyzed with the help of Optical microscopy and SEM. Through microstructure examination, it is found that the filler ERNiCrMo-3 employing for both CCGTA and PCGTA contains the secondary phases enriched with Mo, Nb and Ni. On the contrary ER2553 filler gives the Widmannstetter austenitic, inter-granular austenite and grain boundary austenite structures in the weldments. Due to balanced ferritic-austenitic ratio is analyzed at the fusion zone of ER2553 which shows high hardness. At parent metal of AISI 316L, tensile fractures are observed in all trials of weld joint. [21]

Kangazian and Shamanian (2017) investigated the microstructural and mechanical properties of SAF 2507 and incoloy 825 dissimilar welds by GTAW. The specimen dimensions were 100 mm*50 mm*5 mm using fillers(ER2594 SDSS and ERNiFeCr-1 Ni based super alloy) with the application of PCGTAW and CCGTAW. The weld joints using PCGTAW methods gives finer finer microstructure, lack of Cr-rich phase formation and lower ferrite contents. Incoloy 825 failed the tensile testing in all cases. By using ER2594, weld joints results into higher hardness and lower toughness as compared with ERNiFeCr-1filler metal. According to the results, PCGTAW employing with ERNiCr-1 gives the best mechanical and microstructural properties [22].

Wang (2012) studied the effect of welding process on the mechanical and microstructure properties of dissimilar weldments between duplex stainless steels and low alloy steel. In this experiment, the base metal dimension are taken to be 200 mm*100 mm*8 mm and groove angle is 60°. TIG and MIG welding process are employed with ER2209 wires. More austenite present in the weld metal by MIG than in TIG gives better micro structural properties. Tensile strength of all weld metal are same. Toughness of DSS base metal is higher than wed metal. In the weld metal, MIG gives higher impact toughness as compared to Tig [23].

Ramkumar et al. (2016) studied the effect of fillers on the mechanical and microstructural behaviour of Nb stabilized austenitic stainless steel welds. In this experiment, the thickness of

AISI 347 is 6.67 mm and employing ER347, ER2553 and ERNiCrMo-3 filler materials which can by produced by multi-pass pulsed current gas tungsten arc welding. The microstructure in fusion zone of AISI 347 with filler ER2553 and ERNiCrMo-3 results into dendritic and columnar grain growth. On the contrary, vermicular delta ferrite was analyzed in AISI 347 weld joints fusion zone. The tensile failure is observed in the fusion zone of AISI 347 employing ER2553 and ER347 weld joints and on the parent metal of ERNiCrMo-3 weld joints [24].

Mukesh and Sharma (2013) studied the mechanical properties in AISI 202 stainless steel using GTAW. In this experiment, sample size 100*50*6 mm is taken and the influence of three input parameters (gas flow rate, welding speed and welding current) are investigated by using L9 orthogonal array of Taguchi's methodology and ANOVA. From the analysis, the current has the maximum influence on the tensile and micro hardness of the weld metal. Microstructure shows that the weld metal has delta ferrite structure in the matrix of austenite as well consist in HAZ and parent metal [25].

Reddy et al. (2017) studied the influence of welding parameters on mechanical and micro structural properties of dissimilar ferritic-austenitic stainless steel welds. In this experiment, three welding techniques (GTAW, EBW and Friction welding) are compared. For GTAW and EBW, the hot rolled annealed 20 mm thick sheets is used and in friction welding 20 mm diameter is used of the same material. In GTAW, ER 430 filler material is used and rest are autogenous welds. According to the microstructure, in GTAW welding coarse columnar grains, are observed. On the contrary in EBW, austenitic stainless steel side consists of equiaxed grains and ferritic side contains columnar grains. In friction welding, epitaxial solidification was observed on ferritic stainless steel side and no such feature is observed on opposite side. Electron probe micro analysis shows that inter diffusion of elements was indicative, intermediate in EBW and is not relevant in friction welding. Impact and notch strength of friction welding (consist of ferritic side and dissimilar austenitic ferritic side) is superior than GTAW and EBW. On the austenitic side of EBW exhibited superior notch and impact strength. GTAW shows the lowest pitting corrosion compared to other techniques [26].

Qi and Song (2010) studied the interfacial structure of the joints between mild steel with nickel and magnesium alloy as interlayer by hybrid laser TIG welding. The joint shear strength is improved with the use of interlayer. In this experiment, at the joint interface Ni interlayer is analyzed. The tensile shear strength increases with the Ni interlayer compared to without

interlayer due to the formation of a solid solution of Ni in Fe and intermetallic compound (Mg_2Ni) at the interface [27].

Liu et al. (2006) observed the microstructure og dissimilar welds of Al and Mg alloy with Ce as an interlayer produced by laser-TIG hybrid welds. In this experiment, the Mg and Al alloy thickness used is 1.7 mm. Cracks are not observed in the critical region of the weld joint using Ce as an interlayer. The Ce is uniformly distributed in the critical region at the major region of weld joint of Al alloy and Mg alloy [28].

Babu et al. (2007) studied the correlation of mechanical and micro structural properties of Ti-6Al-4V weldments produced by with and without TIG current pulsing. In this experiment, 1.9 mm thick plate of Ti-6Al-4V is used in the form of α-β processed and mill annealed state. In this study, the room temperature hardness, microstructure and tensile properties of Ti-6Al-4V weldments are observed at room temperature, 150°C, 300°C and 450°C. After that PWHT is applied at 900°C. There is a little refinement of β grains which leads to higher ductility, higher hardness and higher tensile strength. The PWHT at 900°C leads to the strength reduction and improvement in ductility for both pulsed and unpulsed weldments [29].

Choudhary et al. (2014) investigated the design optimization of GTAW welding process parameters by Taguchi Method. In this experiment, Stainless steel (90mm×25mm×4mm) and mild steel (85mm×21mm×3mm) are used and the working length is taken 10mm. It had been reported that L16 orthogonal array has been used and the factors are categorized at different levels of current, gas flow rate and diameter of filler rod. The dominancy of welding process parameters on ultimate load of weldment is done by signal to noise ratio, ANOVA and graphical plots. It has been concluded that by Anova, no welding parameters affects the ultimate load. By main effect plots, the gas flow rate and current has greater influence than filler rod diameter and confirmatory test also confirms the result [30].

Kumar and Sundarrajan (2009) optimize the process parameters of pulsed GTAW to investigate the mechanical properties of AA5456 Aluminum alloy weld joints. 2.14 mm thick plate of Al-Mg Aluminum that is welded with 5356 filler material is employed in the set-up. It has beem observed that L8 2^7 orthogonal array has been applied at two levels of peak current, base current, welding speed and pulse frequency respectively. The analysis is done by regression and analysis of variance. The optimum condition is found out at peak current 80amp, base current at 40amp, welding speed at 230mm/min and pulse frequency 4Hz. The mechanical properties resulted into good improvement at this optimum condition [31].

Lenin et al. (2010) optimize the process parameters of dissimilar weld joints in Arc welding process. In this study, stainless steel 304 and low carbon steel are welded. The L9 3^3 orthogonal array has been employed and factors are categorized into welding speed, current and voltage. The analysis is done by ANOVA and S/N ratio. It is concluded that S/N ratio gives its best property at welding speed 250mm/min, current at 100 amps and voltage at 30 volts. Moreover, the welding current is more dominant factor by ANOVA. By confirmatory test, tensile properties are improved [32].

Juang and Tarng (2002) optimize the process parameters of weld pool geometry in GTAW for stainless steels. In this experiment, the SS304 plates are used of 15mm thickness and single pass welding is done on it. The L16 4^4 orthogonal array is used and the factors are categorized as arc gap (mm), gas flow rate (l/min), welding current (amps) and welding speed (cm/min). The orthogonal array is employed to analyze the weld pool characteristics like back height, back width, front width and front height of weld pool. The quality characteristics is analyzed by S/n ratio and ANOVA. From the applied techniques, the four factors are affecting the multiple quality characteristics and the optimum conditions is simplified. Confirmatory tests shows that weld pool geometry is greatly improved [33].

2.2 LITERATURE GAP

1) From the literature it can be observed that lot of studies related to the effect of corrosion of dissimilar weldment have been done.

2) Combination of Austenitic/ ferritic and austenitic/super alloy containing Fe and Ni weldment are not studied on the basis of micro structural and mechanical grounds.

3) Few studies related to the microstructural and mechanical properties of dissimilar weldment with the combination of austenitic/ferritic, austenitic/Ni based super alloy and austenitic/Fe based super alloy have also been reported

4) However no results has been reported regarding the dissimilar welding of SS 316L austenitic and SS 410 martenistic steel using TIG followed by optimizing welding parameters using L18 orthogonal array.

5) The effect of parameters such as type of groove and the varying fillers ER347, ER 308L and ERNiCrMo- 3 has not been yet analyzed.

Hence, the present investigation focus on analyzing the effect of varying welding parameters such as grooves, current, gas flow rate, arc length and the filler material of welding using

GTAW process of two dissimilar steels. Microstructure observation has been done to check the effect of these parameters on the weld bead. Mechanical test such as tensile strength and micro hardness were also carried out.

2.3 EXPERIMENTAL PLAN

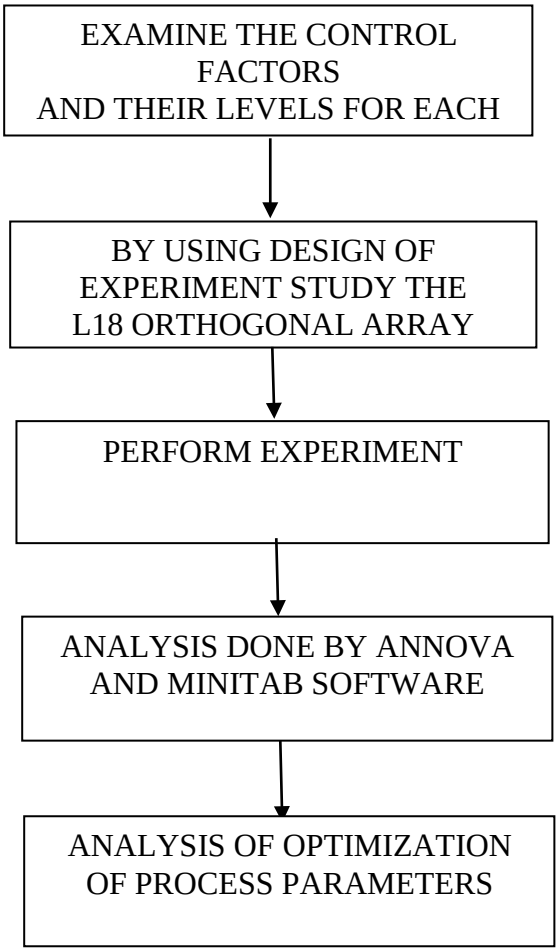

Figure 2.2: Flow chart of experimental plan

Chapter-3

Design of Experiment

By studying the literature review, it can be concluded that with any change in welding parameter, the properties of welding gets affected. So, any change in welding parameter affects the microstructure and mechanical properties of the weldment. The dissimilar weldment (SS316 and SS410) having the combined dimensions of 152mm×100mm×6mm is used as a base metal.

3.1 Examination of base metal elements

Absorption Spectrometry is used to analyze what percentage of element is present in the base metal. Here the spectrometer is used to check the percentage of elements in SS316 and SS 410.

Figure 3.1 Absorption spectrometer (Courtesy: Advance measurement lab, Thapar University, Patiala)

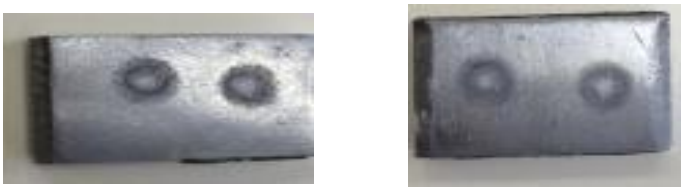

(a) (b)

Figure 3.2: (a) Spectroscopy image of SS 316 (b) Spectroscopy image of SS 410

Table 3.1: Composition of SS410and SS316

Parent metal	C	Cr	Mn	Ni	Si	Mo	P	S	Fe
SS410	0.1428	12.5	1.009	8.53	1.0	-	0.04	0.014	Balance
SS316	0.079	16.68	1.93	12.0	1.0	2.50	0.450	0.030	Balance

3.2 Equipment set-up

Taguchi experiment are performed on Gas Tungsten Arc Welding machine (Techno weld MDX-300) which is available in the central workshop of Thapar University.

In the GTAW, the basic requirements are Tungsten electrode, Power Source, Gas Cylinder, Flow meter, regulator, filler rod, Work piece and connecting cables. The power source is used to provide DCEN, DCEP and AC voltage and current also. The tungsten electrode is a non consumable type of electrode. Gas cylinder is used for argon or helium gas and a flow meter is used to control the flow of a gas.

Figure 3.3: GTAW machine (Courtesy: Welding lab, Thapar University, Patiala)

3.3 PILOT EXPERIMENTS

In order to investigate the dominant factors that will be responsible for change in response parameters, pilot experiment were conducted on the GTAW machine. In the pilot

experiments, first grooves are taken. These grooves are half V, full V and double V. By choosing the grooves, depth of penetration is analyzed. In this experimentation, half v is not filling the root gap completely as well as sometimes this problem is occurring in Full V at the temperature range of 170-230 Amps with the varying gas flow rate 18-25 L/min. Different fillers were also used. There is a problem of wide HAZ as shown in the figure.

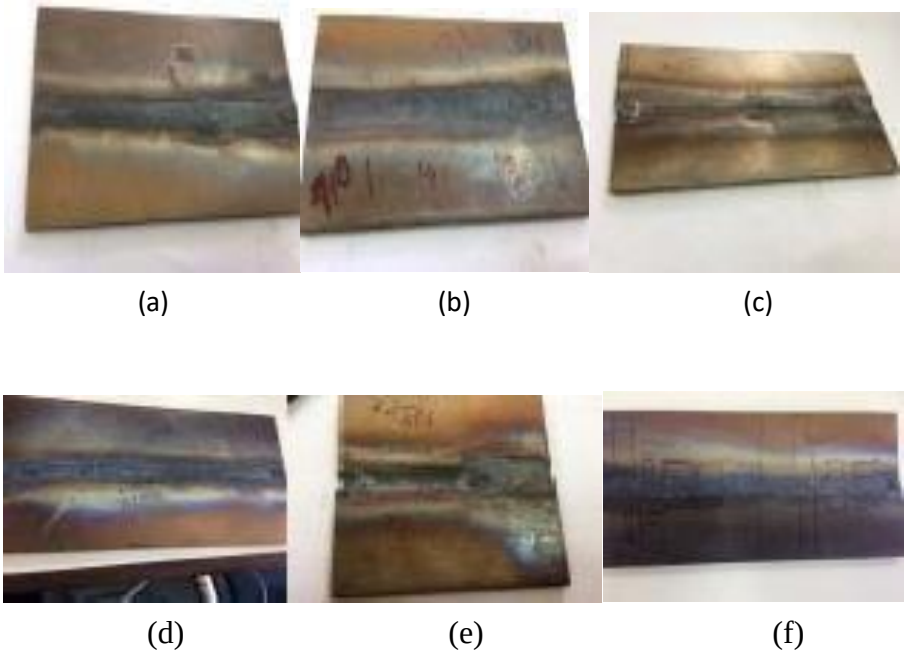

(a) (b) (c)

(d) (e) (f)

Figure 3.4: (a) HAZ of double V groove at 170 Amp, 24 L/min, ER 347 filler with short arc length, (b) HAZ of full V groove at 180 Amp, 22 L/min, ER 308 filler with short arc length, (c) HAZ of full V groove at 200 Amp, 21 L/min, ER 308 filler with short arc length, (d) HAZ of double V groove at 210 Amp, 24 L/min, ER 308 filler with short arc length, (e) HAZ of double V groove at 210 Amp, 24 L/min, ER 308 filler with short arc length, (f) HAZ of double V groove at 210 Amp, 24 L/min, ER 308 filler with short arc length

3.4 SELECTION FOR ORTHOGONAL ARRAY

In this study, the four factors are varied at three levels and one factor varied at two levels. The formula of degree of freedom is N-1 (N represent the number of levels). The degree of freedom for three levels is 2 and for two level is 1. Therefore, the total number of degree of freedom is 9. So, orthogonal array L18 is chosen.

Table 3.2: Table for computing degree of freedom

SERIAL NO.	PARAMETER	UNITS	DEGREE OF FREEDOM
1	ARC LENGTH	Mm	1
2	CURRENT	Amp	2
3	FILLER MATERIAL	-	2
4	TYPE OF GROOVES	-	2
5	GAS FLOW RATE	L/min	2
6	**TOTAL**		9

3.5 ORTHOGONAL ARRAY

The Taguchi method is used for reducing the variation that comes in a process through the design of experiment. Its main objective is to generate the goods at low cost and high quality to the manufactures. In Japan, Dr. Genichi Taguchi introduce the concept of design of experiment. Foe the selection of appropriate orthogonal array for experiments, the total degrees of freedom should be calculated. The number of comparisons in the taken parameters that must be employed to evaluate which level and parameter is optimum and best and especially by how much is defined as degrees of freedom. The two level process parameter is examined for one degree of freedom. The degree of freedom due to the interaction of two parameters is evaluated by the multiplication of degrees of freedom of two process parameters. If once the degree of freedom is known, then orthogonal array can be designed to fit the determined task. The degree of freedom of orthogonal array is only justified when degree of freedom is greater than or at least equal to the process parameters. In this experiment, L18 orthogonal array with 5 columns and 18 rows were used. The process parameters are associated with columns and rows indicates the 18 welding process parameters were examined. The 18 combinations of process parameters are taken in the entire welding process space. The L18 orthogonal array is illustrated below in table

Table 3.3: Orthogonal array

EXPERIMENT NO.	ARC LENGTH	CURRENT	FILLER MATERIAL	TYPE OF GROOVES	GAS FLOW RATE
1	SHORT	180	ER 308	HALF V	20
2	SHORT	180	ER 347	FULL V	23
3	SHORT	180	ERNiCrMo-3	DOUBLE V	25
4	SHORT	200	ER 308	HALF V	23
5	SHORT	200	ER 347	FULL V	/25
6	SHORT	200	ERNiCrMo-3	DOUBLE V	20
7	SHORT	220	ER 308	FULL V	20
8	SHORT	220	ER 347	DOUBLE V	23
9	SHORT	220	ERNiCrMo-3	HALF V	25
10	LONG	180	ER 308	DOUBLE V	25
11	LONG	180	ER 347	HALF V	20
12	LONG	180	ERNiCrMo-3	FULLV	23
13	LONG	200	ER 308	FULLV	25
14	LONG	200	ER 347	DOUBLE V	20
15	LONG	200	ERNiCrMo-3	HALF V	23
16	LONG	220	ER 308	DOUBLE V	23
17	LONG	220	ER 347	HALF V	25
18	LONG	220	ERNiCrMo-3	FULL V	20

3.6 SAMPLE PREPARATION

As we require different type of groove as stated in above table so, we need to fabricate these different samples. These edge preparation work for different grooves was performed with the help of power hacksaw and surface grinding machine.

Figure 3.5: Welded sample specimen

Power hacksaw was used to cut the sample into desired dimension and surface grinder was used to grind the edge into desired shape.

Figure 3.6: Power hexa (Courtesy: Central tool workshop, Thapar University, Patiala)

Figure 3.7: Surface grinder (Courtesy: CNC lab, Thapar University, Patiala)

3.7 DISCRIPTION OF FACTORS USED

3.7.1 Filler material

The filler wires are used for root layer for tacking and filling between the root gap of the three types of grooves are ER308L, ER347 and ERNiCrMo-3. The chemical composition of these fillers are given below

Table 3.4 Composition of filler material

Filler wire	C	Si	Ni	P	S	Mn	Cu	Cr	Nb	Mo
ER 308L	0.02	0.3-0.65	9.0-11.0	.03	.03	1-2.5	0.75	19.5-22.5	-	0.75
ER 347	0.04	0.40	9.50	0.025	0.015	1.30	0.10	19.50	0.40	0.30
ERNiCrMo-3	0.10	0.5		0.02	.015	0.5	0.5	20.0-23.0	-	8-10

Table 3.5 Properties of filler material

Filler wire	Ultimate Tensile strength	Elongation	Yeild strength
	Kgf/mm^2	%	Psi
ER 308L	52-65	35-45	57000
ER 347	52-64	42	88000
ERNiCrMo-3	76-80	30-35	115000

3.7.2 Types of grooves

In this experiment, the included angle is taken 60°. The types of grooves are Half V groove, Full V groove and Double V groove.

(a) (b) (c)

Table 3.8 (a) double V, (b) half V, (c) full V

3.7.3 Arc length

In this study, the two arc length are taken i.e. short and long arc length. The short arc length is near about 0.5mm-1.5mm and the long arc length is 2.5mm-3.5mm.

3.7.4 Current

In this study since current is varied at three level so three value of current in this investigation are 180 Amp, 200 Amp and 220 Amp.

3.7.5 Gas flow rate

As in case of current gas flow rate is also varied at three level and the values of gas flow rate in this investigation are 20 L/min, 23 L/min and 25 L/min.

3.8 EQUIPMENT USED IN TESTING

Different testing were done after the experimentation of all the trails obtained from orthogonal array which are listed below

3.8.1 Universal tensile testing machine

Tensile testing is done at MNNIT Allahabad using BISS_25KN machine (Model No ASTM E8-09). It is the ratio of maximum load that a material can withstand without being get fractured when it is stretched to the original cross sectional area of the material. When the stresses less than that of tensile strength are removed then the material partially or completely return to its original shape and size. If the stresses applied is equal to the tensile strength of that material, then material flow through a narrow, constricted zone and easily get fractured. Tensile strength is defined as the force per unit area.

Figure 3.9: Universal tensile testing machine (Courtesy: MNNIT, Allahabad)

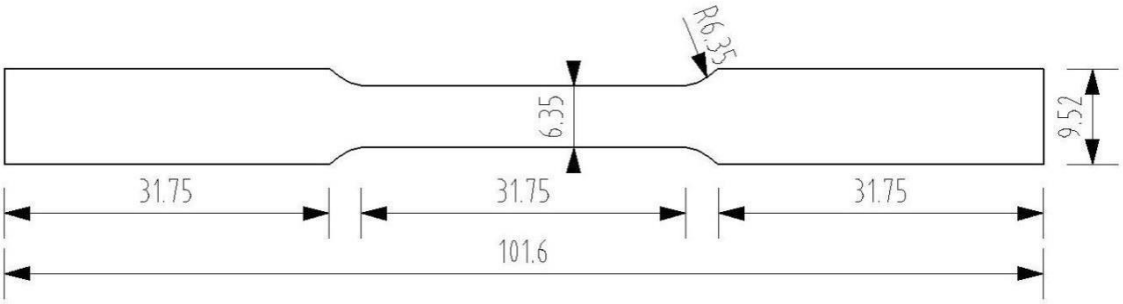

Figure 3.10: Schematic diagram of tensile sample

Figure 3.11: Tensile sample

The samples prepared for tensile testing were prepared according to American Section of the International Association for Testing Materials (ASTM) standard.

3.8.2 Micro hardness tester

Measurements were done on a computer Interfaced Micro Hardness Tester (Model: MVH2), available at Thapar University, Patiala. Micro hardness is defined by the diamond point indenter that penetrates to microscopic areas. For measuring the micro hardness, the samples should be polished so that the micro structures should be visible on the lens of the micro hardness tester. Firstly, the samples are finished on the belt grinder. Then, these samples are rubbed with emery paper of 220, 400, 600, 800, and 1000 and then polished on the disc polisher as shown in the figure below. Micro hardness of the weld bead, the interface of beads on both sides and the both parent metal are computed by the computer that is interfaced by micro hardness tester. The measurements were dependent on size of indentation of the

given samples. With the use of Quantimet software at 40X magnification, the diagonals of indentations are formed designated by pyramid shaped diamond indenter which gives direct vickers micron hardness number. The load applied on the samples are 300gm for 20 sec dwell time.

Figure 3.12: Micro hardness testing machine Model: MVH2 (Courtesy: Advance Measurement Lab, Thapar university, Patiala)

3.8.3 Optical microscopy

Optical microscope also termed as light microscope or leica microscope, which utilizes visible light and a set of lens to see the magnified images. These are the oldest type of microscope which was invented in 1917 basically used to see microstructures. In this analysis, first the samples are polished and can be seen at 10X lens. On seeing by the microscope, the samples microstructures is seen in the computer attached to the microscope. From the computer where the image is developed, the image is then saved. These samples are first polished at belt grinder, then emery paper ranging from 220, 400, 600, 800, 1000, 2000 and last is polished by alumina of fine 1 micron size.

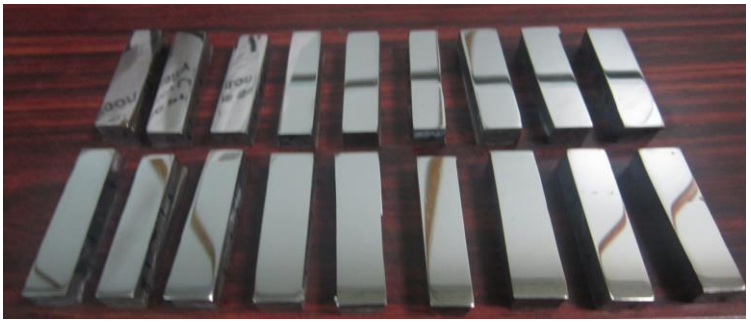

Figure 3.13: Polished specimen for optical microscopy

Figure 3.14: Leica microscopy (Courtesy: Advance measurement lab, Thapar University, Patiala)

Figure 3.15: Disc polisher (Courtesy: Metrology lab, Thapar University, Patiala)

3.8.4 Field emission scanning electron microscope

In FESEM high energy electron focus beam used for generate different variety signals to get information about sample morphology, chemical composition, and crystalline structure. The SEM used for this study is a highly accurate and precise instrument.

Figure 3.16: FESEM machine model no. Merlin Compact -6073(Courtesy: Central University of Bathinda, Bathinda)

3.9 ANALYSIS OF VARIANCE (ANOVA)

ANOVA is a statistical tool which can draw important conclusions based on the analysis of the outcome experimental data. The method helps in revealing the level of significance of influencing factor or the interaction of factors on the particular response. It evaluates the total variability of the response (sum of the square deviations about the grand mean) into contributions rendered by each of the parameter/ factor and the error. Thus

SST = SSF + SSE

Where, SST=$\sum_{k=1}^{n} (\gamma_k - \gamma_m)^2$

Where, SST = Total sum of squared deviations about the mean.

γ_k= Mean response for j[th] experiment.

γ_m = Grand mean of the response.

SSF = Sum of squared deviations because of each factor.

SSE = Sum of squared deviations caused due to error.

In the ANOVA table mean square deviation is defined as:

MS = Mean Square

MS = $\frac{SS\,(Sum\ of\ the\ squared\ division)/}{DOF(Degree\ of\ Freedom)}$

F-value is the Fisher's F ratio (Variance ratio) expressed as:

F= $\frac{MS\ for\ a\ factor/}{MS\ for\ the\ factor\ error\ )}$

Depending on F value, P-value or probability of significance is used to be calculated. If the P-value for a factor appears less than of 0.05 (For 95% confidence level) then it can be analyzed that the influence of the factors / interaction of given factors is significant on the given or taken response. Significance of all the dependent variables can be evaluated by using statistical software MINITAB 15. The dependent variables are to be analyzed in this study are (1) Tensile strength (2) Micro hardness.

In the ANOVA table, the DOF or degrees of freedom are used to evaluate the mean squares (MS). In general, the degrees of freedom signifies how much the "independent" information is available to evaluate each sum of squares (SS).

Total DOF = DOF for all the factors + DOF for all the interactions + DOF for the error

Where n signifies the total number of observations and,

DOF for factor = k−1

Where k indicates the count of the factor levels.

DOF for the Interaction = (k1−1) × (k2−1)

Where k1 is the count of levels of factor one and k2 is the count of levels of factor two. The same rule is applied to the interactions of more than two factors. In the present study, the interaction of given factors has not been analyzed. The sequential sum of squares for the each factor in the model evaluate the amount of variation that is present in the response which is explained by adding the each factor to the model sequentially in the order listed under. Thus, the sequential sums of the squares for factors are specific that develop a linear model between the factors. The adjusted sum of square for a factor in the model (factor or interaction) evaluate the amount of the additional variation in the outcome response that is illustrated by the factor, illustrate that all the other factors are already in the model. Thus, the data for the adjusted sums of squares are independent of the order of the interactions listed under given source. The adjusted mean squares for the term is generally the adjusted sum of squares (Adj. SS) which is divided by the degrees of freedom [22].

CHAPTER-4

RESULTS AND DISCUSSIONS

4.1 TENSILE TEST RESULTS

Tensile tests are carried out on ultimate tensile testing machine. Ultimate tensile strength for SS316 is generally 620-795 MPa and SS410 is 485-690 MPa. The tensile samples were prepared on the set standards on ASTM E8-09 which can give acceptance test. The readings are to be taken out by using different parameters.

The specimens which are broken in tensile tests are shown in Fig 4.1

Figure 4.1: Broken specimen from tensile test

For the experimental work, the response parameter is higher the better. The all tensile test are shown in the table 4.1. The graph of corresponding load versus displacement and stress versus strain shown below

Table4.1: Maximum Tensile Load and Maximum Tensile Strength at various process parameters

Experiment No.	Contributing factors	Maximum tensile load(KN)	Maximum Tensile strength(MPa)
1	A1,C1,F1,G1,R1	17.306	692.255
2	A1,C1,F2,G2,R2	18.696	747.834
3	A1,C1,F3,G3,R3	17.919	716.756
4	A1,C2,F1,G1,R2	17.135	685.381

5	A1,C2,F2,G2,R3	22.41	896.388
6	A1,C2,F3,G3,R1	17.641	705.621
7	A1,C3,F1,G2,R1	18.996	759.849
8	A1,C3,F2,G3,R2	17.365	694.611
9	A1,C3,F3,G1,R3	17.332	693.265
10	A2,C1,F1,G3,R3	16.518	660.726
11	A2,C1,F2,G1,R1	9.826	393.024
12	A2,C1,F3,G2,R2	16.945	677.809
13	A2,C2,F1,G2,R3	18.184	727.355
14	A2,C2,F2,G3,R1	17.868	714.706
15	A2,C2,F3,G1,R2	11.898	475.916
16	A2,C3,F1,G3,R2	14.203	568.122
17	A2,C3,F2,G1,R3	15.688	627.5
18	A2,C3,F3,G2,R1	17.686	707.432

Where,

- A represents the arc length and varied at two levels namely A1 is the short arc length and A2 is the long arc length.
- C represents the current and varied at different levels where C1 is 180 Amperes, C2 is 200 Amperes and C3 is 220 Amperes.
- G represents the types of grooves at three different levels where G1 stands for half V, G2 for Full V and G3 for Double v groove.
- F represents the types of filler material at different levels where F1 stands for ER 308, F2 for ER 347 and F3 stands for ERNiCrMo-3.

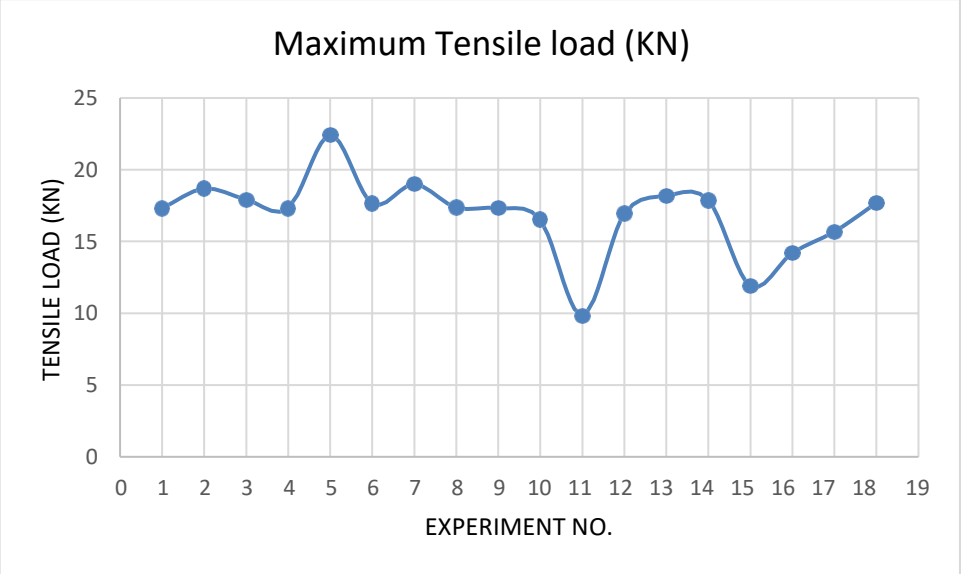

Figure 4.2: Graph of maximum tensile load at different experiment process parameters

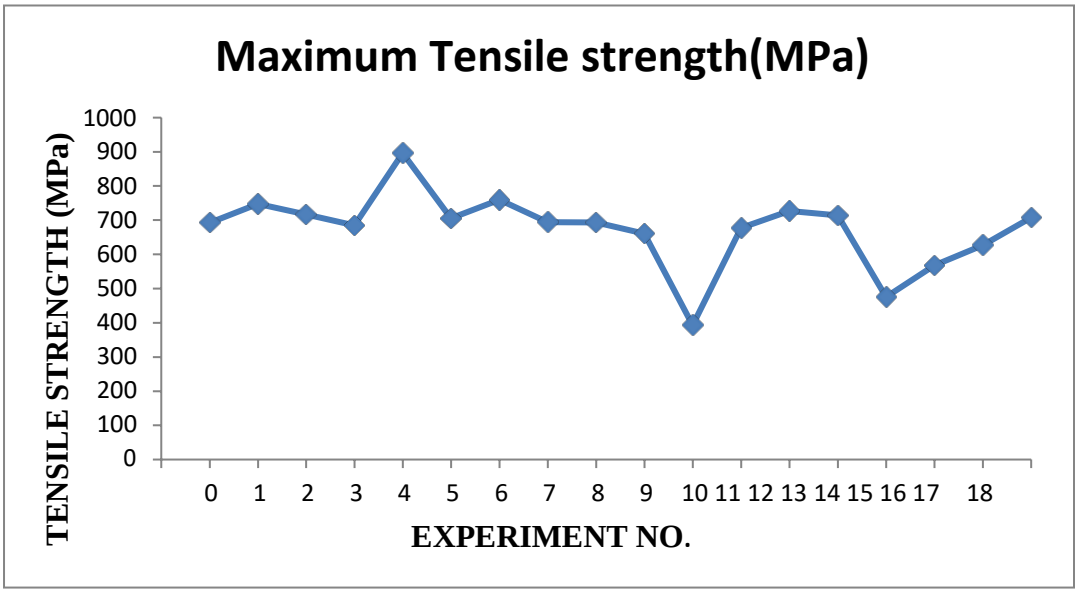

Figure 4.3 Graph of Maximum Tensile Strength at various experiment process parameters

For the experimental work, the response parameter is higher the better. The all tensile test are shown in the table 4.1. The graph of corresponding load versus displacement and stress versus strain shown below

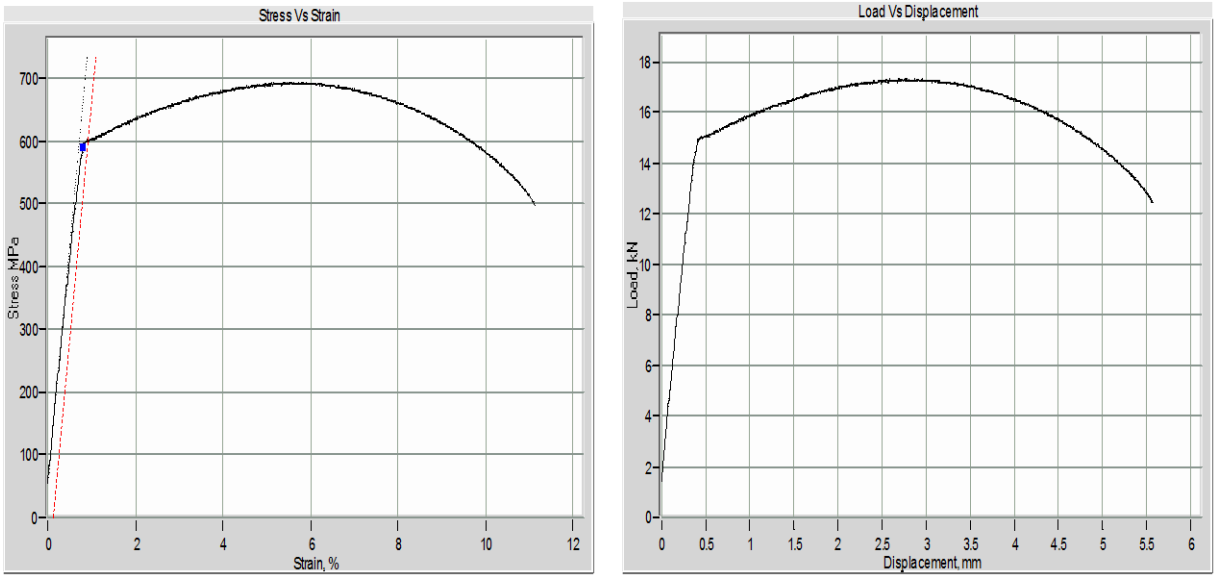

(a) (b)

Figure 4.4: (a) Stress vs Strain curve for trial 1 (b) Load vs Displacement curve for trial 1

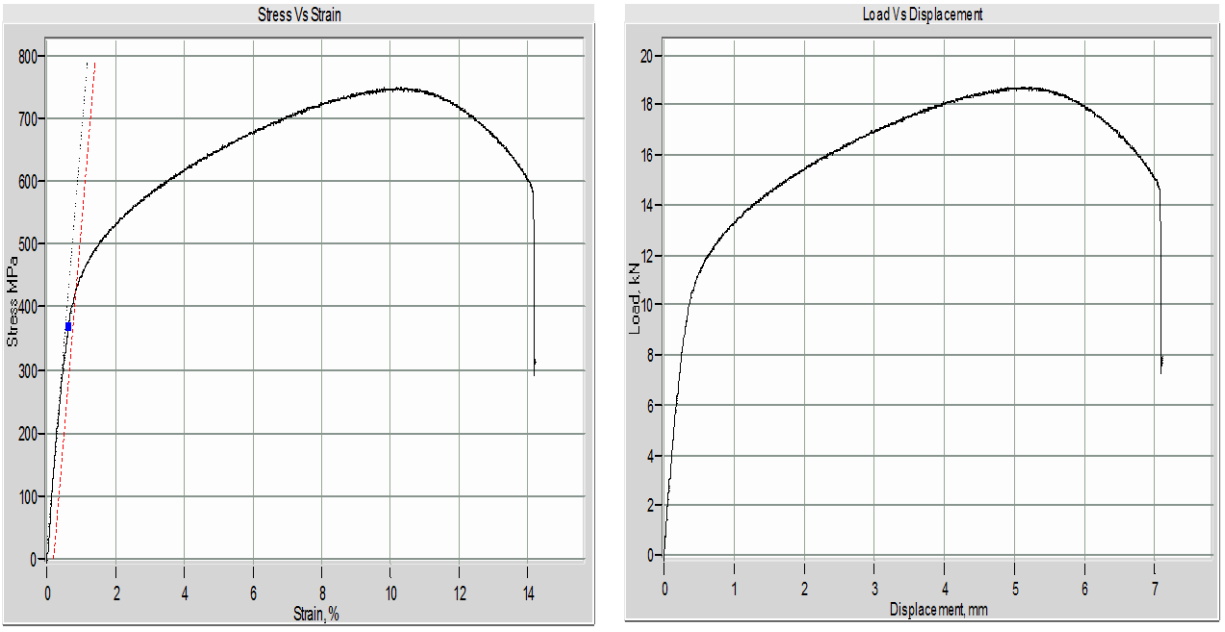

(a) (b)

Figure 4.5: Stress vs Strain curve for trial 2 (b) Load vs Displacement curve for trial 2

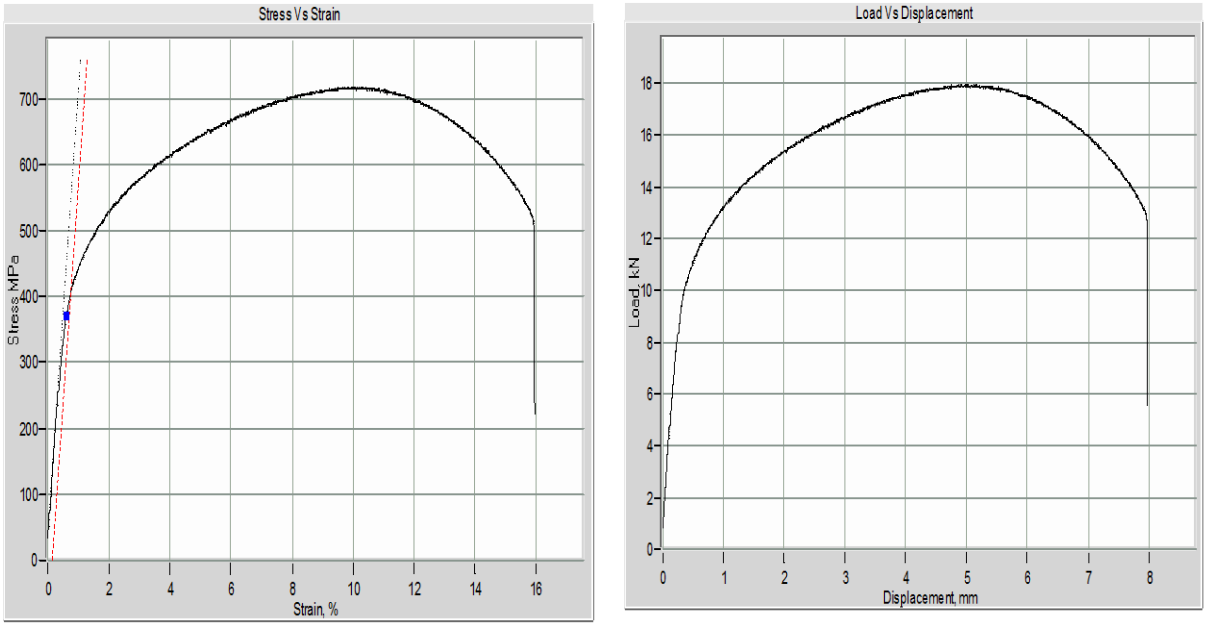

(a) (b)

Figure 4.6: (a) Stress vs Strain for trial 3 (b) Load vs Displacement curve for trial 3

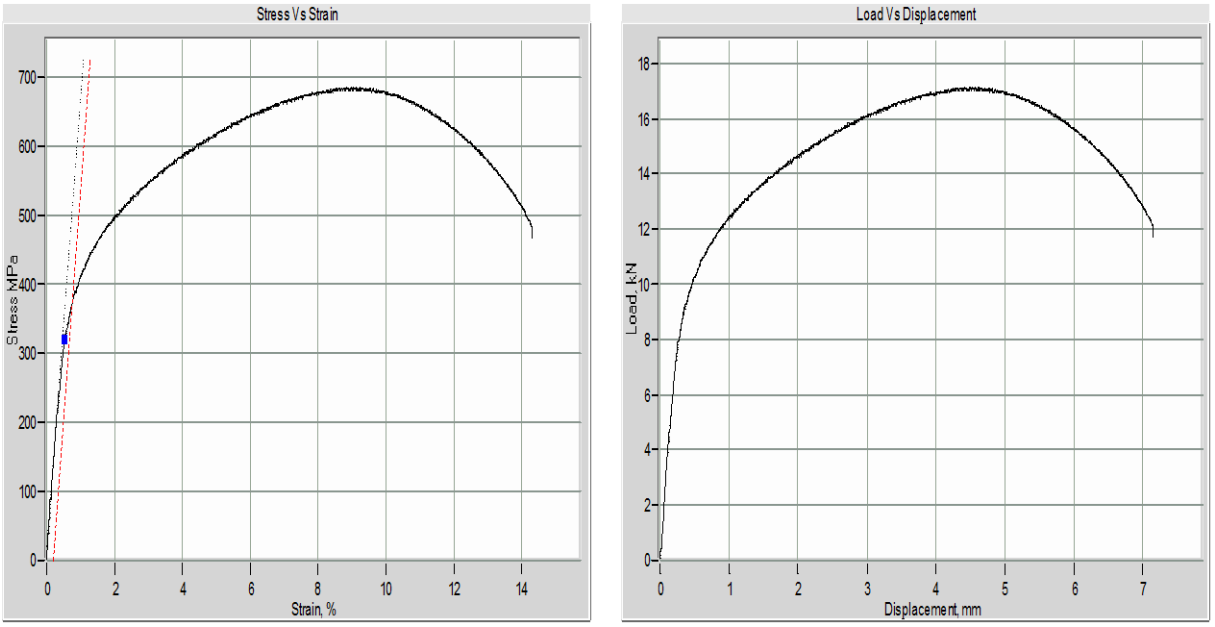

(a) (b)

Figure 4.7: (a) Stress vs Strain for trial 4 (b) Load vs Displacement curve for trial 4

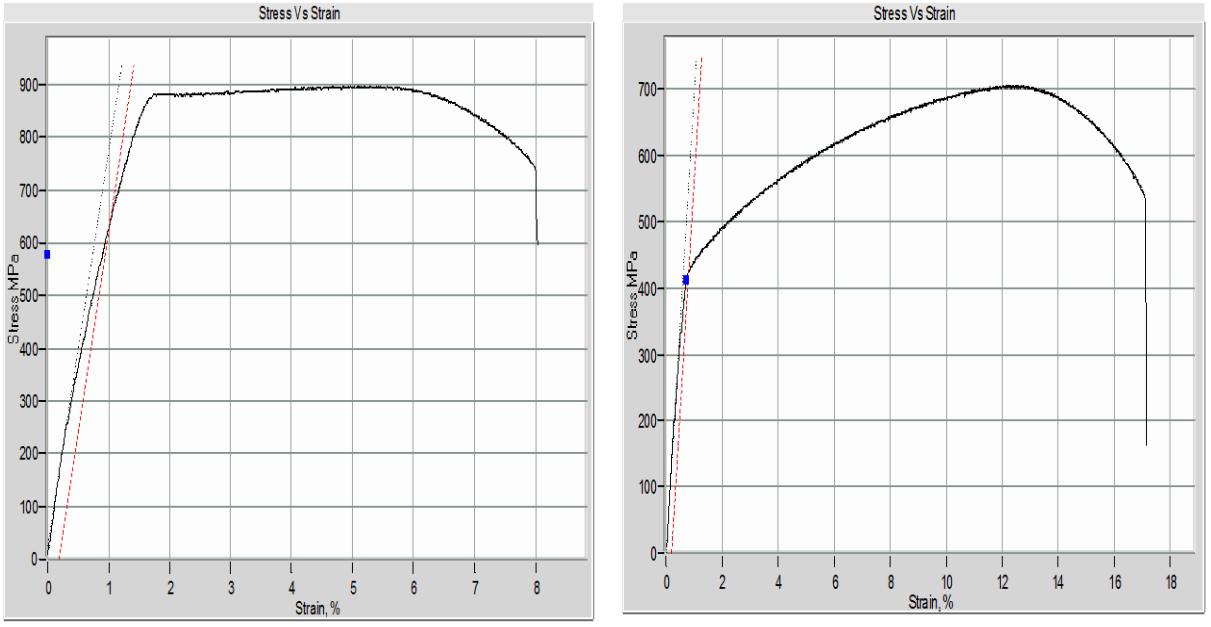

(a) (b)

Figure 4.8: (a) Stress vs Strain for trial 5 (b) Load vs Displacement curve for trial 5

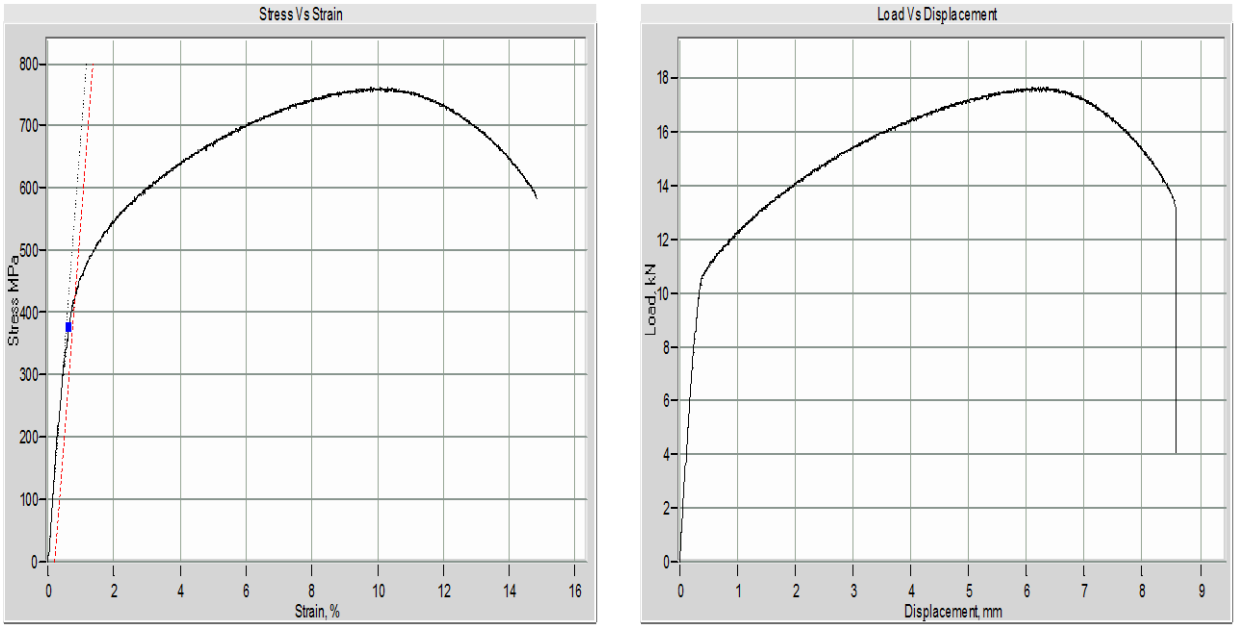

(a) (b)

Figure 4.9: (a) Stress vs Strain for trial 6 (b) Load vs Displacement curve for trial 6

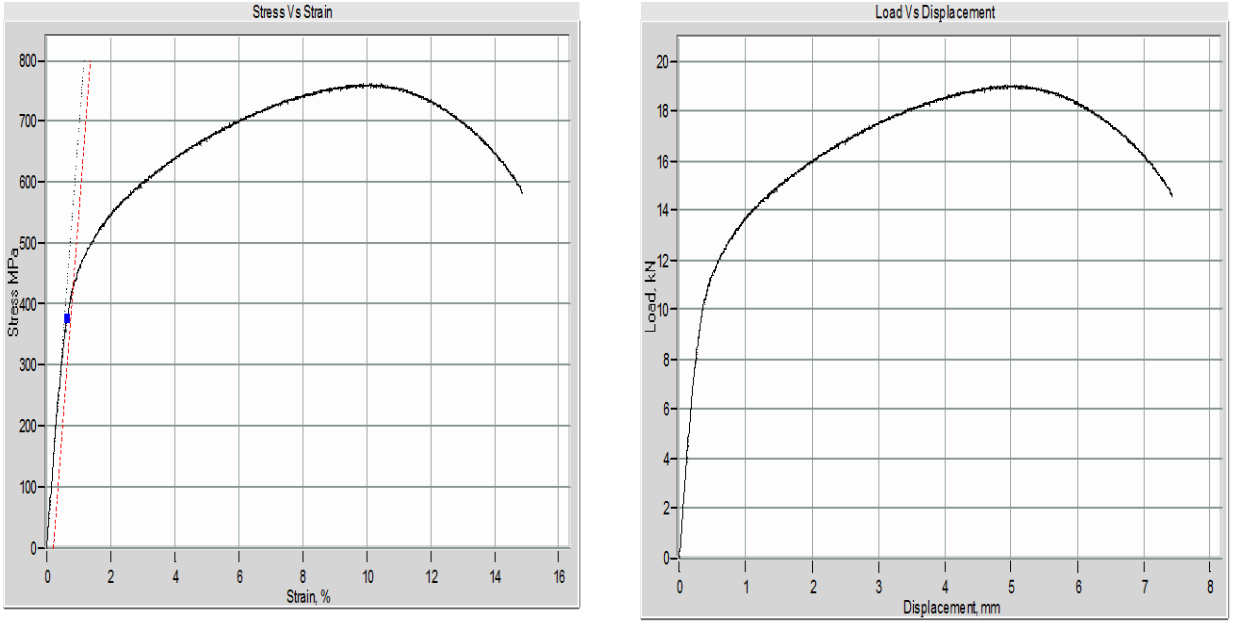

(a) (b)

Figure 4.10: (a) Stress vs Strain for trial 7 (b) Load vs Displacement curve for trial 7

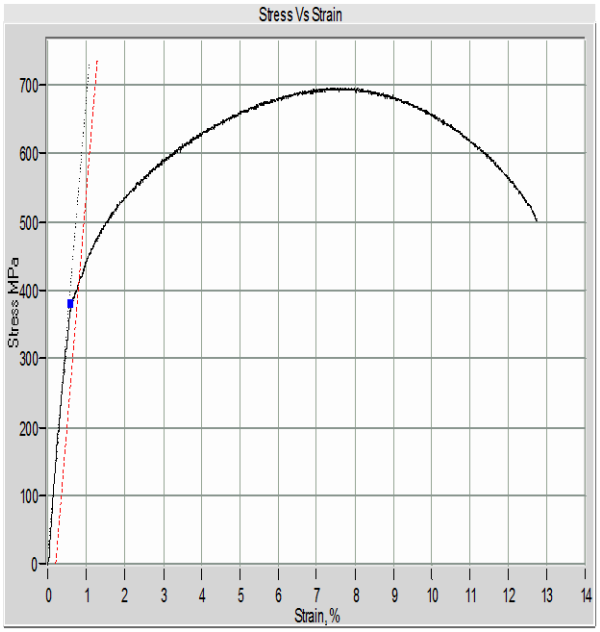

(a)

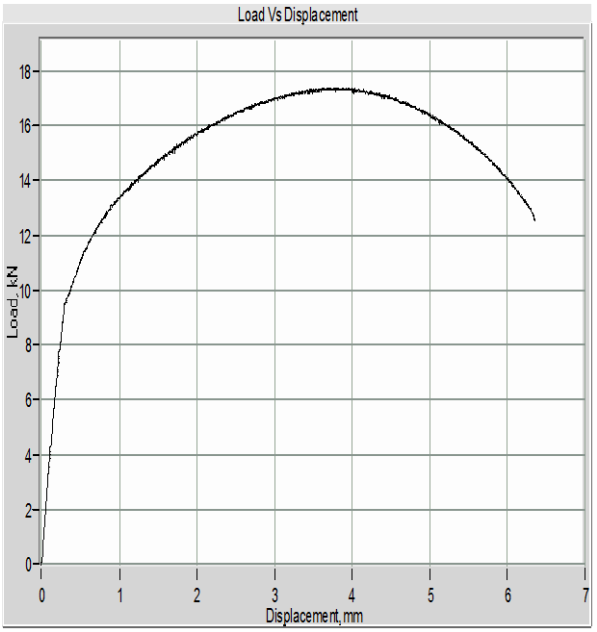

(b)

Figure 4.11: (a) Stress vs Strain for trial 8 (b) Load vs Displacement curve for trial 8

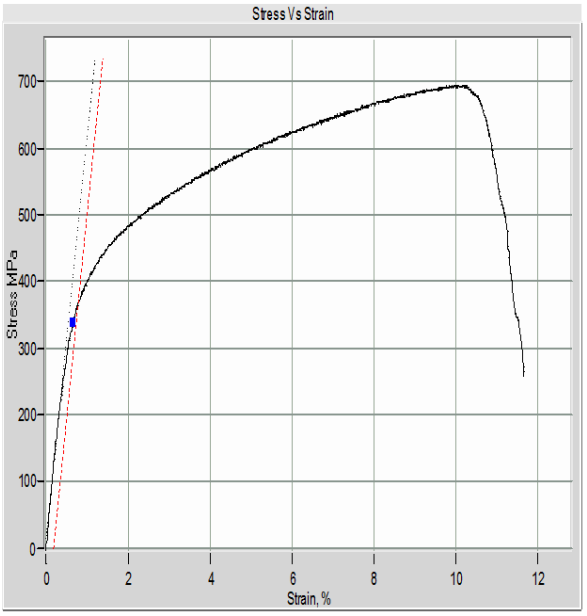

(a)

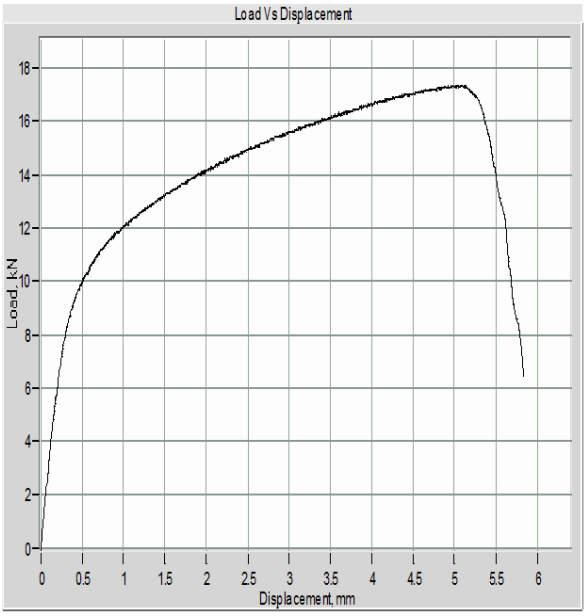

(b)

Figure 4.12: (a) Stress vs Strain for trial 9 (b) Load vs Displacement curve for trial 9

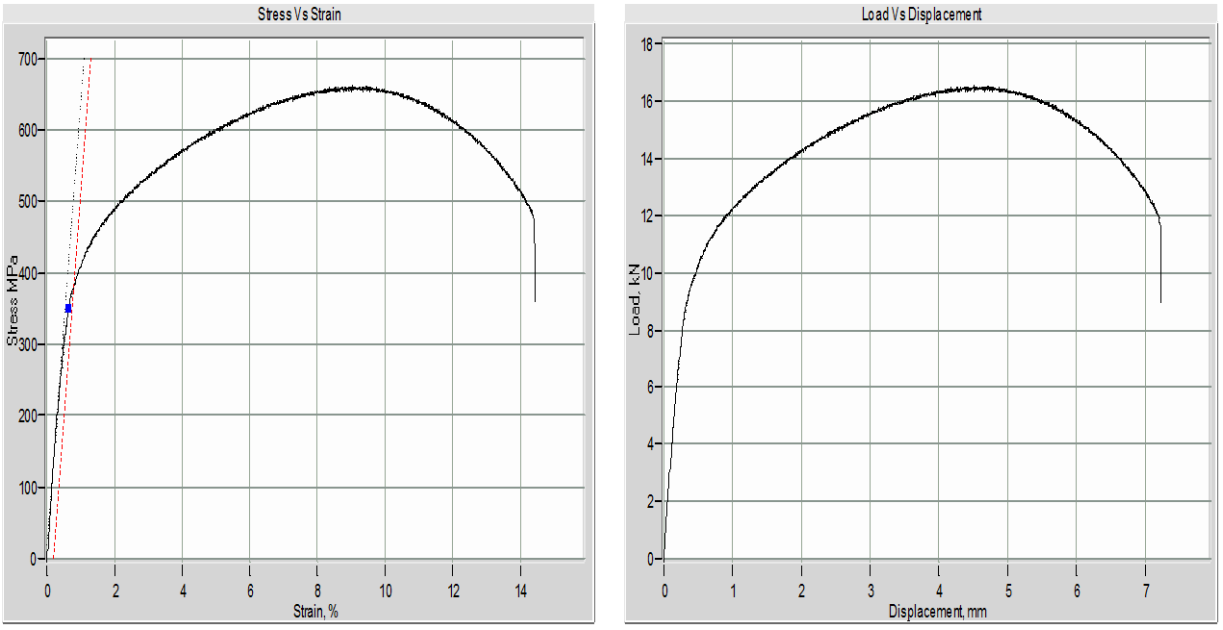

(a) (b)

Figure 4.13: (a) Stress vs Strain for trial 10 (b) Load vs Displacement curve for trial 10

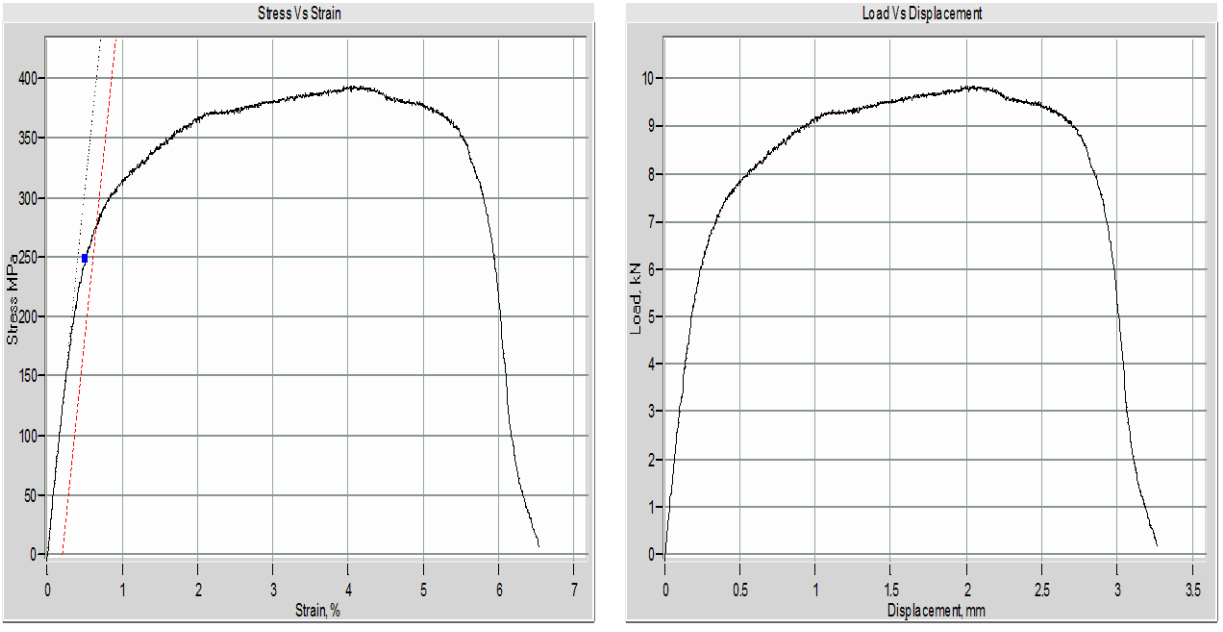

(a) (b)

Figure 4.14: (a) Stress vs Strain for trial 11 (b) Load vs Displacement curve for trial 11

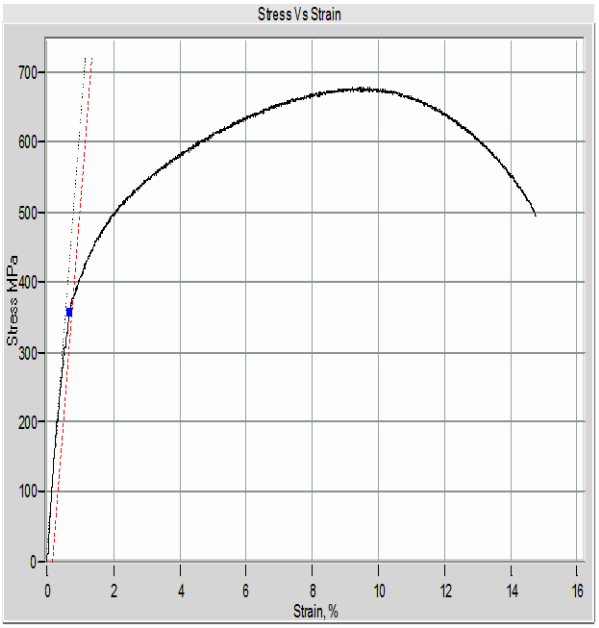

(a)

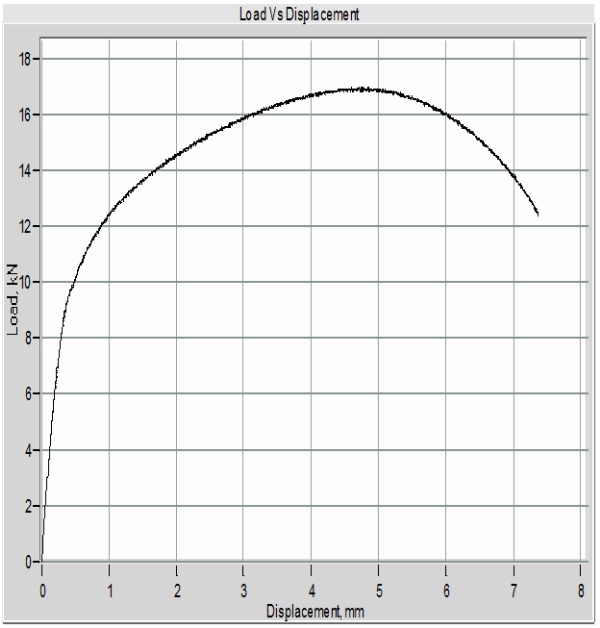

(b)

Figure 4.15: (a) Stress vs Strain for trial 12 (b) Load vs Displacement curve for trial 12

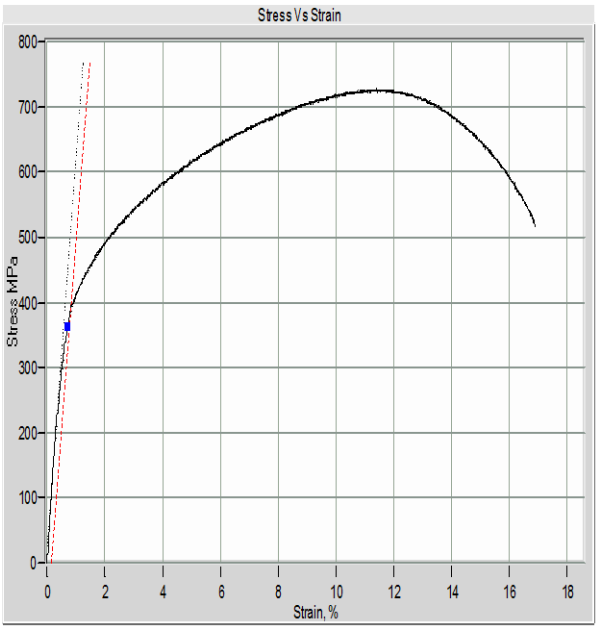

(a)

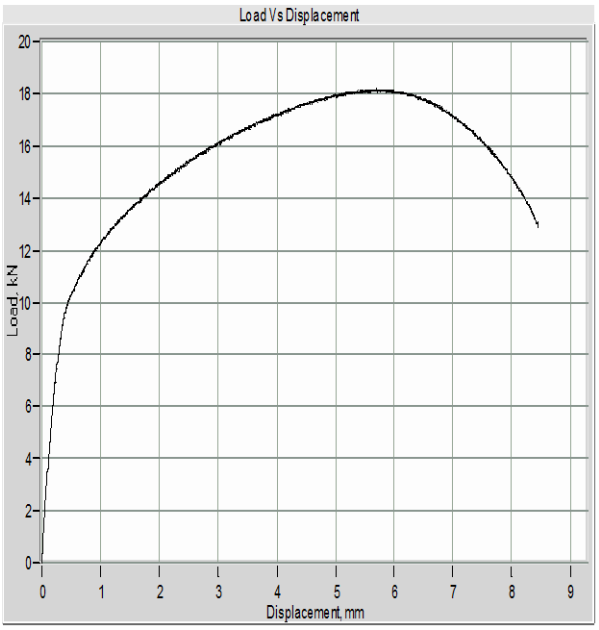

(b)

Figure 4.16: (a) Stress vs Strain for trial 13 (b) Load vs Displacement curve for trial 13

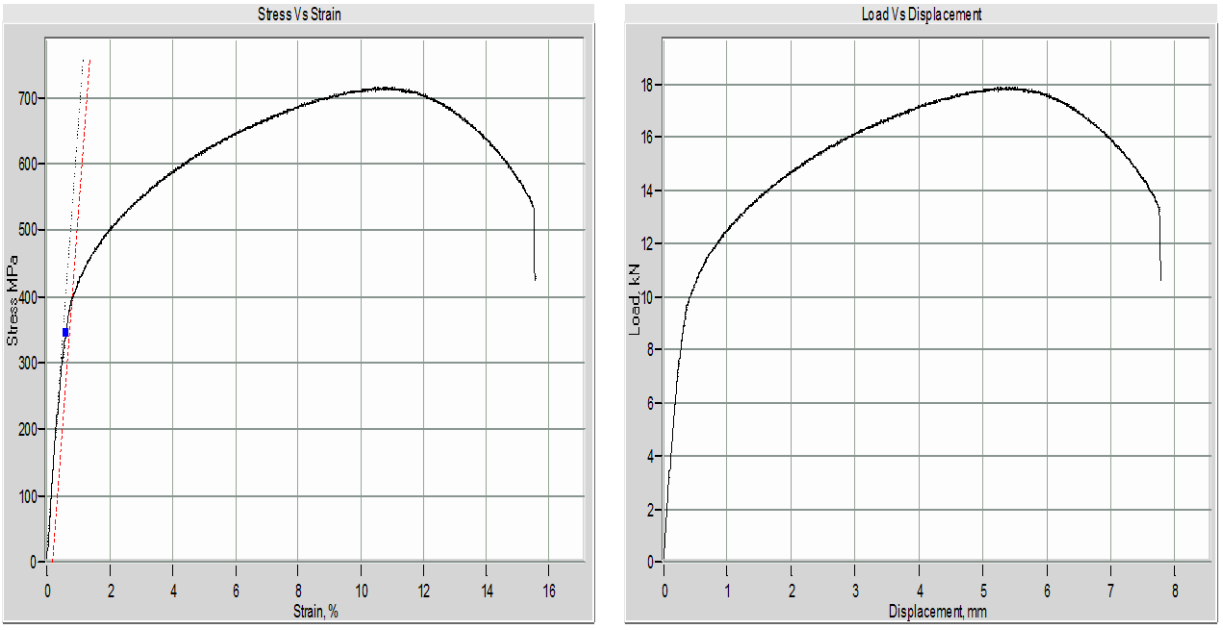

(a) (b)

Figure 4.17: (a) Stress vs Strain for trial 14 (b) Load vs Displacement curve for trial 14

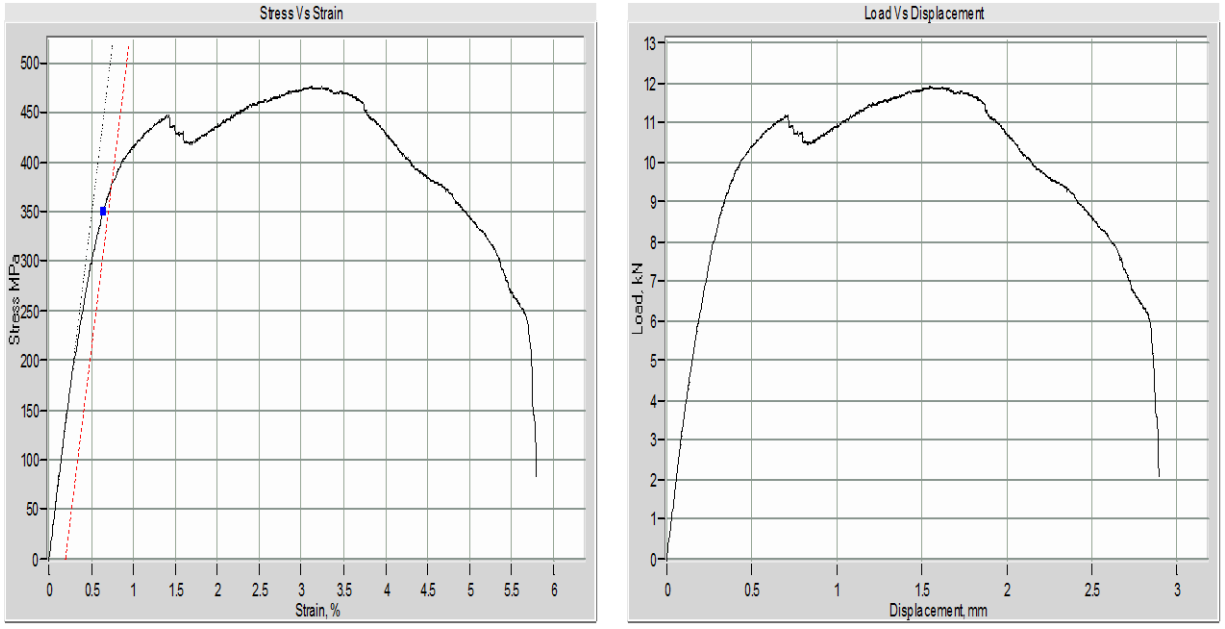

(a) (b)

Figure 4.18: (a) Stress vs Strain for trial 15 (b) Load vs Displacement curve for trial 15

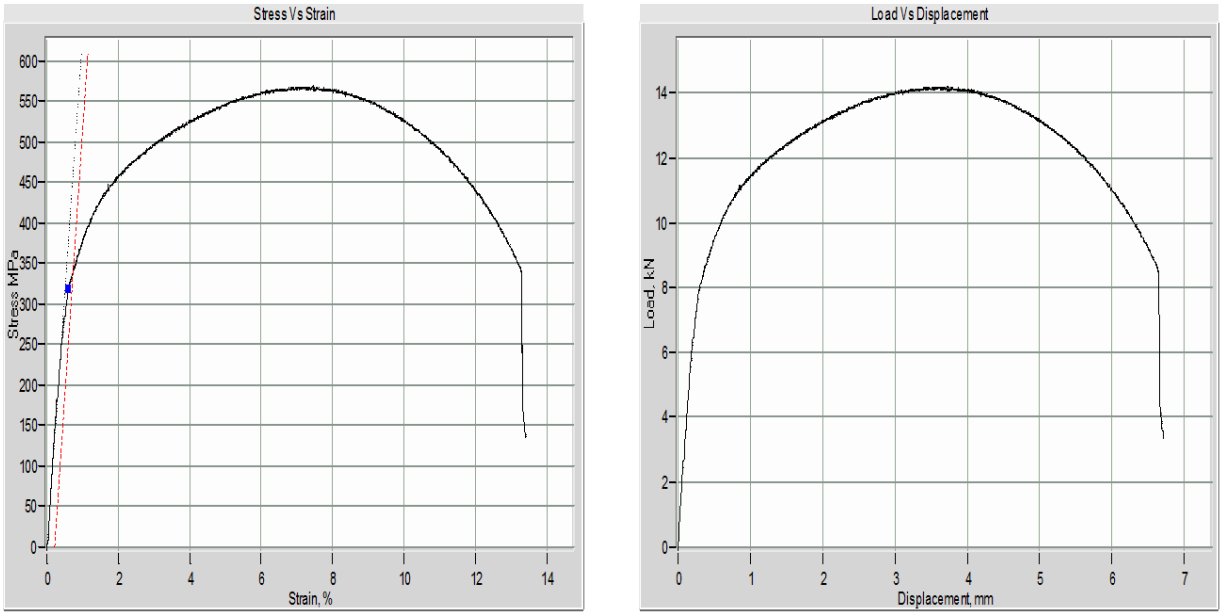

(a) (b)

Figure 4.19: (a) Stress vs Strain for trial 16 (b) Load vs Displacement curve for trial 16

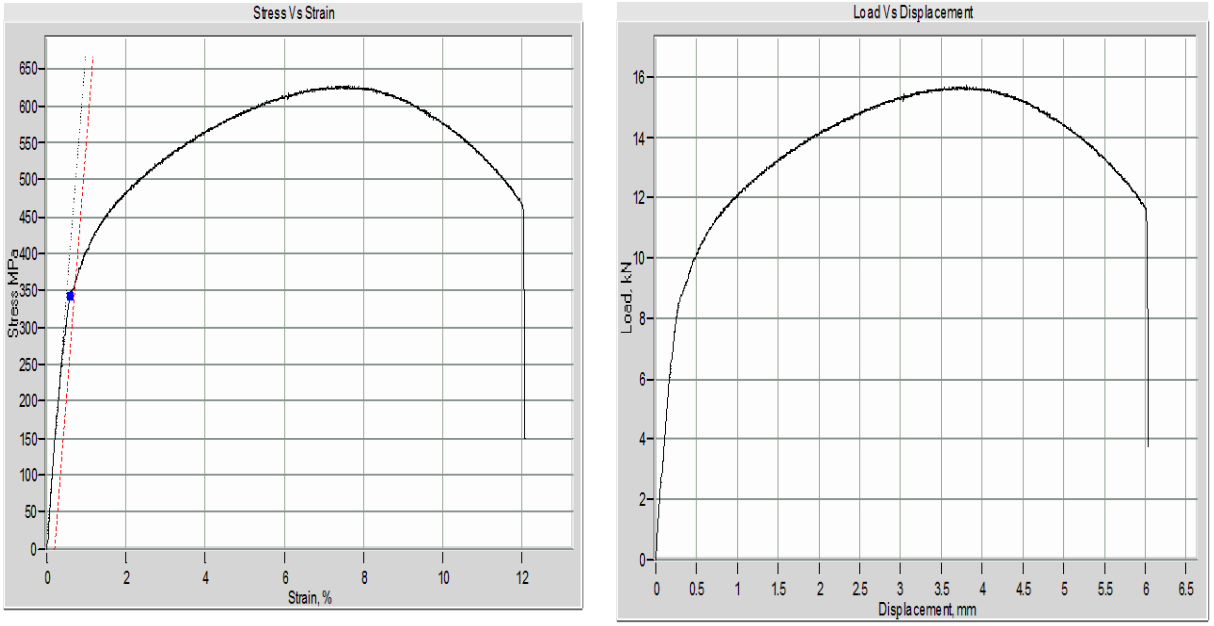

(a) (b)

Figure 4.20: (a) Stress vs Strain for trial 17 (b) Load vs Displacement curve for trial 17

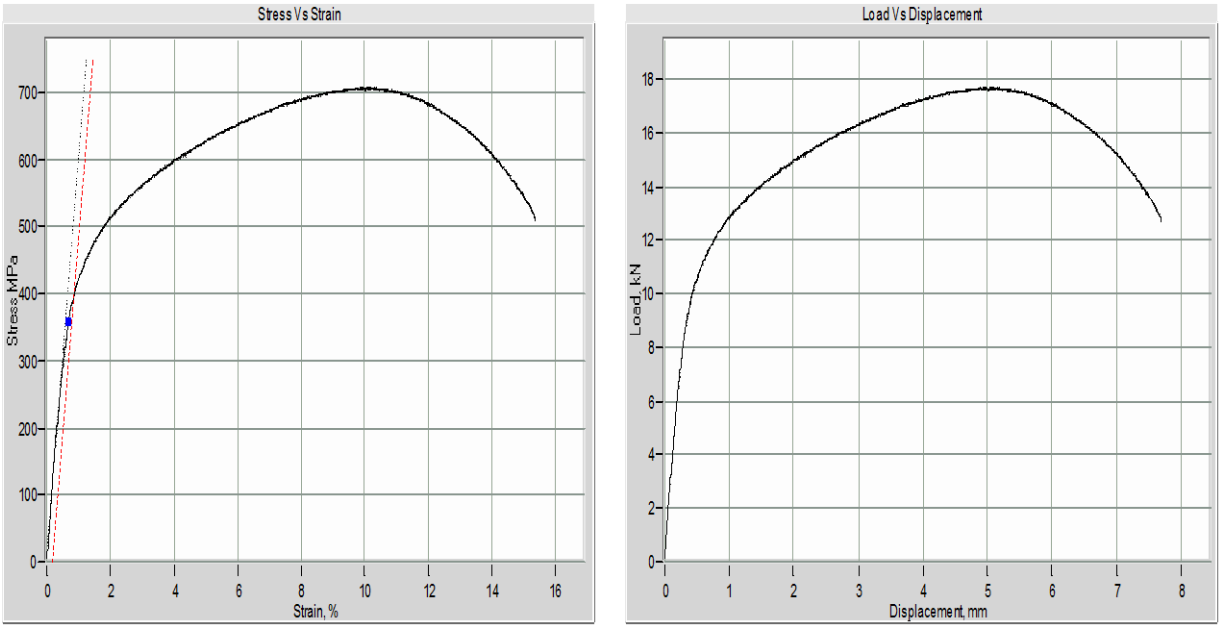

(a) (b)

Figure 4.21: (a) Stress vs Strain for trial 18 (b) Load vs Displacement curve for trial 18

4.2 ANOVA FOR TENSILE STRENGTH

The tensile strengths are shown in eighteen trials that are given in table 4.1. The tensile strength results were evaluated by using ANOVA table. The significance of factors on the desired characteristics can be analyzed in the column of table 4.2 by the p-value. The concept behind the p-value is that the p-value should be less than that of 0.05 (considering the confidence level to be of 95%). From the F-value, it should be larger than the e-pooled, larger the value F-value, more the significant the factors. In ANOVA, from the table it is shown that the arc length is significant factor as p-value less than that of .05 i.e. 0.005 and the second one is types of grooves whose p-value is less than that of 0.011. The mean values for all six variables are shown in table 4.3. From the last column of table 4.3 show the ranks of the factors. Higher the rank leads to more the significance. From the response table for means in table4.3, the most significant factor is types of grooves and the least significant factor is types of fillers used which affects the tensile strength. The variation between in the arc length, current, types of fillers, types of grooves and gas flow rate are discussed in response table for means in table 4.3. The types of grooves from the figure 4.22 shows that there is a increase in tensile strength from double V groove to full V groove and decrease from full V groove to

half V groove. Then the arc length and gas flow rate shows moderate effects on tensile strength and the least effect is shown by the types of fillers.

Table 4.2: Analysis of variance for mean tensile strength

Source	Degree of freedom	Seq SS	Adj SS	Adj MS	F	p
A	1	67142	67141.6	67141.6	14.6	0.005
B	2	11919	11919.3	5959.6	1.30	0.326
C	2	278	278.1	139.0	0.03	0.970
D	2	75792	75792.0	37896.0	8.24	.011
E	2	18902	18902.1	9451.0	2.05	0.191
Residual error	8	36802	36802.1	4600.3		
Total	17	210835				

Table 4.3: Response table for Means

Level	A	B	C	D	E
1	617.0	648.1	682.3	686.8	672.1
2	739.1	710.9	679.0	752.8	641.6
3		675.1	672.8	594.6	720.3
Delta	122.1	62.8	158.2	158.2	78.7
Rank	2	4	5	1	3

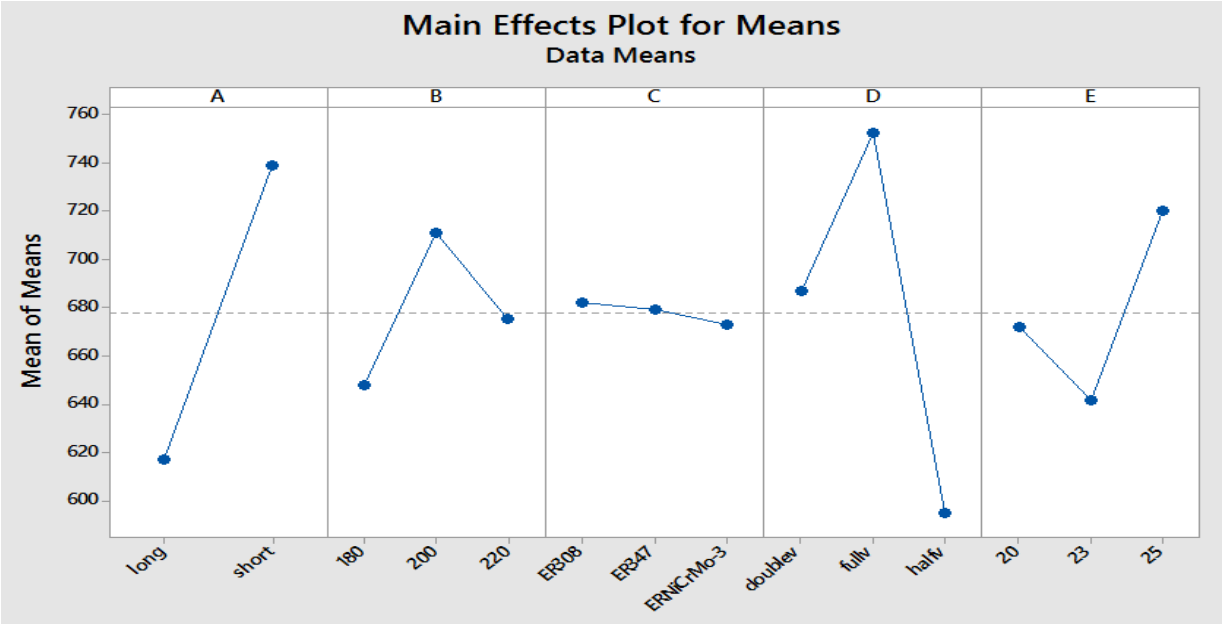

Figure 4.22: Graph for the main effect plot for tensile strength.

4.3 FESEM RESULTS

4.3.1 Sample image of 7th trial

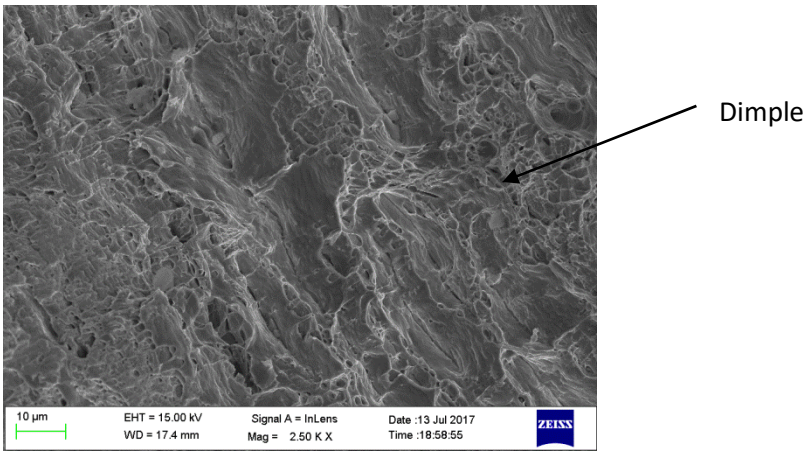

Figure 4.23 FESEM image of 7th trial

This SEM image comprises the factors including short arc length, current 220 Amps, filler 308L, groove Full V and gas flow rate is 20L/min. Ductile fracture with the tensile load associated with 18.699 KN and tensile strength associated is 759.849MPa. The dimped shapes on the right side indicates the ductile fracture and on the left side the structure is partly ductile. And the elongation regarding this sample is 14.863%.

4.3.2 Sample image of 11th trial

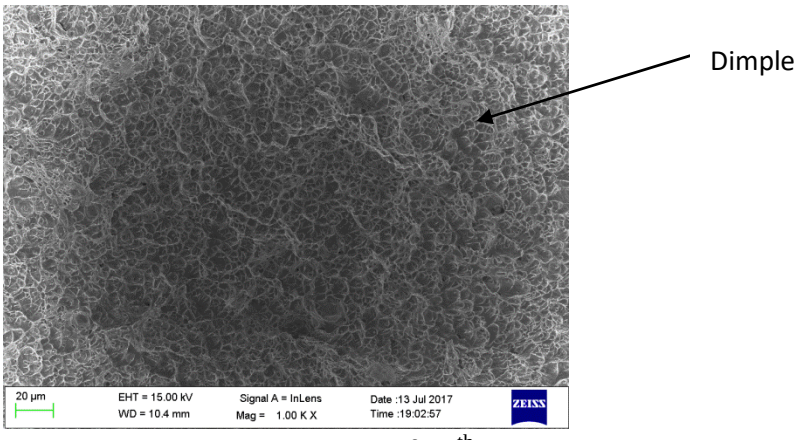

Figure 4.24 FESEM image of 11th trial

The SEM images comprises of the factors long arc, 180 Amps current, Filler ER347, half v groove and gas flow rate is 20L/min. The tensile load applied is 9.826 KN and tensile strength is 393.024 MPa. The fracture shows the ductile fractures as the microstructures are dimpled shaped. The percentage elongation at the break is 6.535.

4.3.3 Sample image of 15th trial

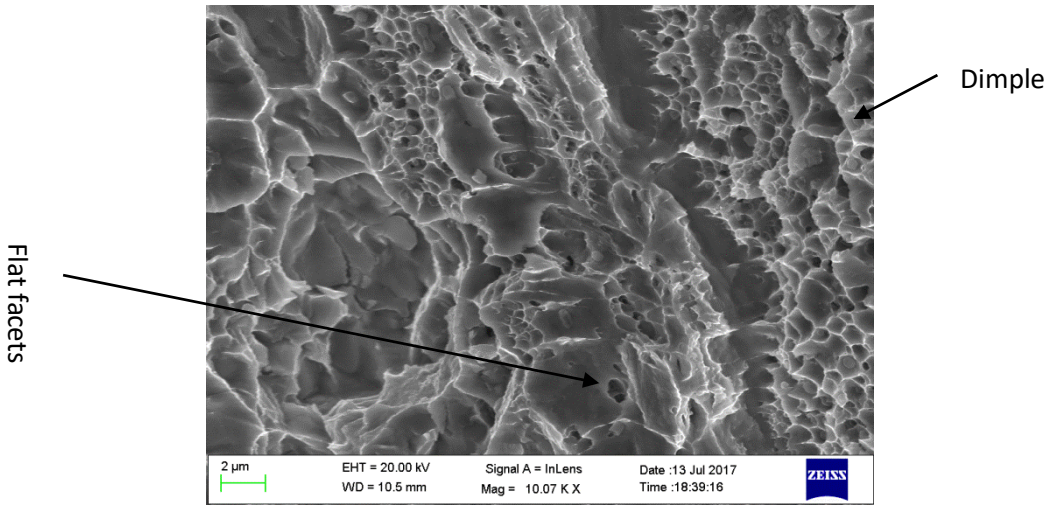

Figure 4.25 FESEM image of 15th trial

This SEM images comprises of long arc, current 220 Amps, filler ErNiCrMo-3, Half V groove and gas flow rate is 23 L/min. The tensile load applied is 11.898 KN and tensile strength 475.916 MPa. On the right side, the dimples on the microstructure is dimple shaped and representing the ductile fracture. In the mid of SEM images there is flat faces are present and the left face is representing partly ductile and brittleness. The percent elongation is 5.796.

4.4 MICRO HARDNESS TEST RESULTS

On the micro hardness tester, the indent load is taken a 300gm and dwell time is 20 sec. For the individual 18 trials, the 5 values are taken in the weld bead area. Then the average is taken of the five values of their respective values.

Table 4.4: Result for micro hardness

EXPERIMENT NO.	Ist trial	2nd trial	3rd trial	4th trial	5th trial	Average Value of 5 trials
1	287.6	296.9	290.8	295.6	300.1	294.2
2	293.2	294.6	280	281.7	282.5	286.4
3	308.8	306.4	293.3	288.3	307.2	300.8
4	288.4	280.4	283.6	292.9	289.7	287
5	283.8	271.7	282.4	269.2	270.9	275.6
6	289.5	287.9	287.1	273.7	269.3	281.5
7	292.7	286.6	283.4	291.4	295.9	290
8	258.1	270.2	271	259.5	272.7	266.3
9	264.4	277.5	259.4	279.9	278.3	271.9
10	296.7	287.4	293.5	284.2	288.7	290.1

11	274.5	275.9	289.1	286.6	287.4	282.7
12	291	290.2	288.6	304.1	309.1	296.6
13	270.7	280	267.5	276.8	275.5	274.1
14	278.9	265.7	268.2	280.3	267.4	272.1
15	265.6	283.7	284.5	270.6	286.1	278.1
16	265.3	271.4	262.1	266.6	274.6	268
17	268.9	258.2	271.4	269.7	256.8	265
18	263.9	277.5	264.4	261.7	282.5	270

4.5 ANOVA FOR MICRO HARDNESS

The ANOVA for the values of micro-hardness can be calculated by using minitab17 software and the p-value should be less than 0.05 so that the factors become significant. The ANOVA should be applied on the average value for micro-hardness of individual experiments.

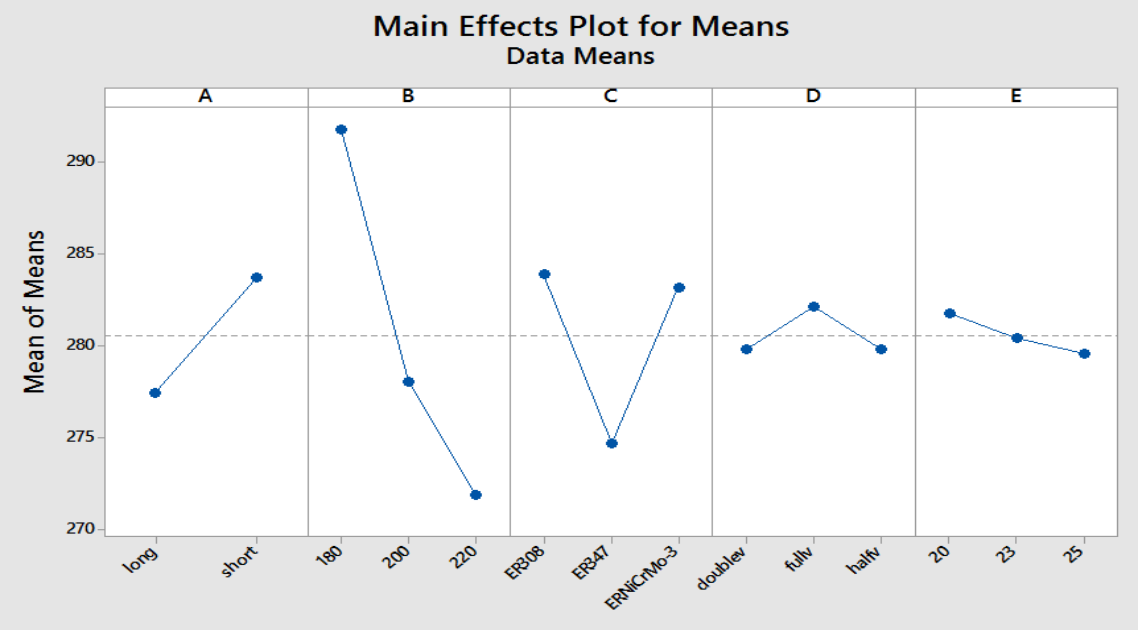

Figure 4.26: Graph analysis for main effect plot for means

Table 4.5 Response table for Means

Level	A	B	C	D	E
1	277.4	291.8	283.9	279.8	281.8
2	283.7	278.1	274.7	282.1	280.4
3		271.9	283.2	279.6	279.6
Delta	6.3	19.9	9.2	2.3	2.2
Rank	3	1	2	4	5

Table 4.6 Analysis of variance for mean micro hardness

Source	Degree of Freedom	Seq SS	Adj SS	Adj MS	F	P
A	1	180.50	180.5	180.500	5.38	.049
B	2	1248.76	1248.76	624.382	18.60	.001
C	2	314.39	314.39	157.194	4.68	.045
D	2	21.31	21.31	10.657	0.32	.737
E	2	14.37	14.37	7.184	0.21	.812
Residual Error	8	268.50	268.50	33.562		
Total	17	2047.83				

According to the Minitab 17, the results were analyzed by the table 4.5 and 4.6. From the table 4.6 it is shown that the dominant factor is current, types of fillers added and the least effect is given by gas flow rate. The moderate effect is given by applying types of grooves and arc length. By the table 4.6 it is seen the significant factors are arc length, current and types of fillers. From the figure 4.26 it is shown micro hardness is decreasing from long arc length to short arc length and current is decreasing from 220 to 200 and slightly from 200 to 180. The effect of fillers are decreasing from ER 308 to ER 347 and increasing to ERNiCrMo-3.

4.6 OPTICAL MICROSCOPY TEST RESULTS

Microstructure, composition and phase study of weld samples as well as parent metal is a another name of metallurgical study. The current study is based on GTAW whose parameters arc length, current, types of fillers, types of grooves and gas flow rates. In this analyzes, dominancy of parameters is examined. Microstructural analysis is done on the basis of shape and type of grain structure, in which manner they are distributed and arranged and their proportion. As the welding is done, due to heat molten metal pool is formed and the grains are recrystallized. As the weld metal is allowed to cool that is the subsequent cooling, there is a change in microstructure is observed. The deciding factors are heat input and cooling rate for the formation of grain size, shape and its properties. Hence optical microscopy is done for microstructural analysis. Here the etchant used is Ralph's etchant. The composition of Ralph's is 100cc H_2O+200cc methyl alcohol+100cc HCl+2gm$CuCl_{2+}$7gr$FeCl_{2+}$5cc HNO_3.

4.6.1 Discussion of Optical microscopy

All microstructures are for the weld bead of different trials.

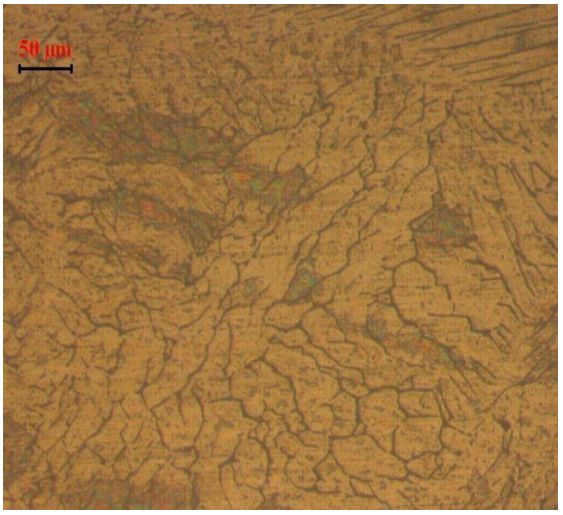

(a)

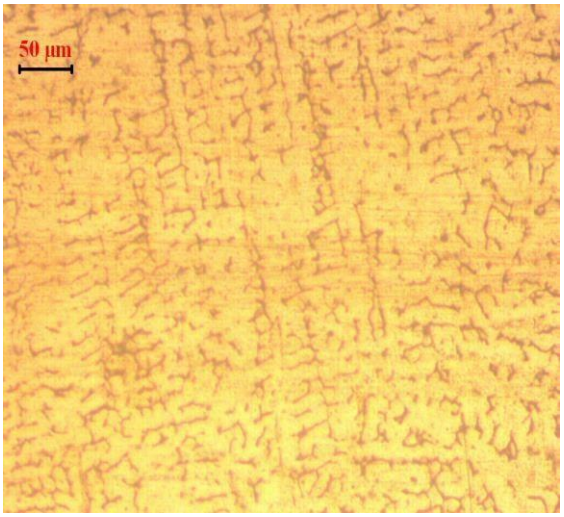

(b)

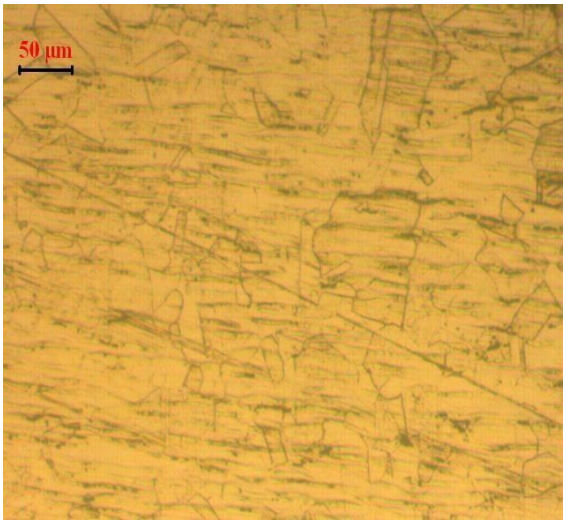

(c)

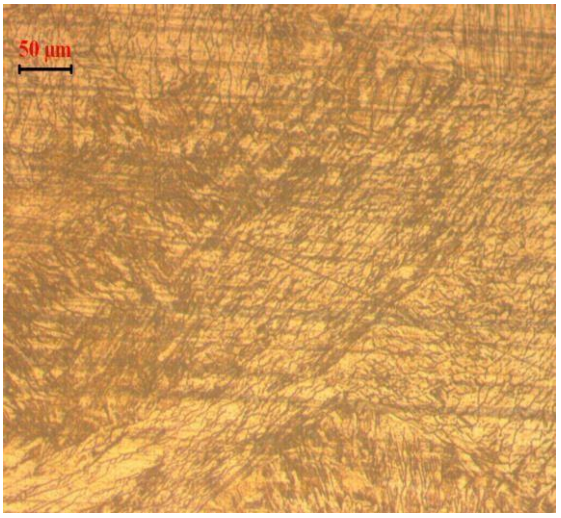

(d)

Figure 4.27: (a) Microstructural image for trial 1 (b) Microstructural image for trial 2 (c) Microstructural image for trial 3 (d) Microstructural image for trial 4

The microstructure on these factors comprises the weld metal consists of compositions contributed by the dissimilar base metals as well as filler material.

For the figure 4.27 (a), the various parameters are taken short arc length, current 180 Amp, filler used is ER308L, half V groove and gas flow rate is 20 L/min. The optical micrograph shows the polygonal shapes of grains. The figure is showing the coarse grain structure too. From the figure 4.27 (b), the various parameters are taken as short arc, current 180 Amp, ER347, full V groove and gas flow rate is 23 L/min. shows the optical micrograph. The weld

metal comprises of black colour and white colour. The black colour comprises δ-ferrite and white portion comprises of austenitic matrix. Morphology of δ-ferrite with Skelton morphology. Few regions also indicates segregation of δ-ferrite within the austenite matrix. For the figure 4.27 (c), the various factors are taken short arc, current 180 Amp, ERNiCrMo-3 filler, Double V and gas flow rate 25L/min. The optical micrograph shows the microstructure of the composite zone i.e. comprising of weld metal, fusion boundary and HAZ zone. The weld metal comprises of ferrite depressed in austenitic matrix and the occurrence of it is inter- dendritic structure. From the figure 4.27 (d), the various factors are taken as short arc, current 200Amps, ER308 L, Half V groove and gas flow rate L/min. In the optical micrograph, the grain coarsening effects clearly seen. Annealing twins can be easily seen.

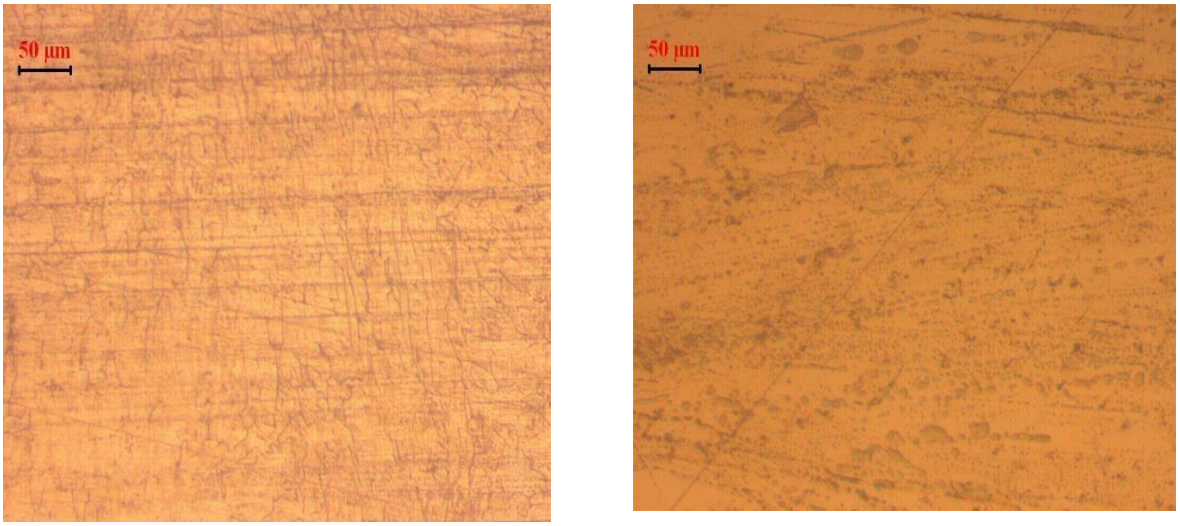

(a) (b)

Figure 4.28: (a) Microstructural image of trial 5 (b) Microstructural image of trial 6

For the figure 5 the various factors are short arc, 200 Amps, ER 347, Full V and gas flow rate 25 L/min. Due to the presence of niobium in ER 347 weld metal ferrite morphological differences are same. Also the ferrite stringers are seen with in the austenitic matrix. For the Figure 6, the various factors are taken short arc, current 200Amps, Filler ERNiCrMo-3, type of groove is Double V and gas flow rate is 25 L/min. From the optical micrograph, weld metal largely comprises of inconel 615 and the contribution of higher nickel content to the weld metal is seen in the form of suppression of ferrite is lesser compared to previous structures.

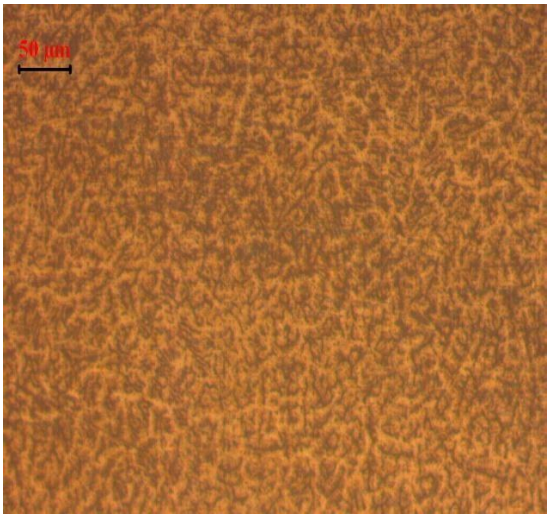

(a)

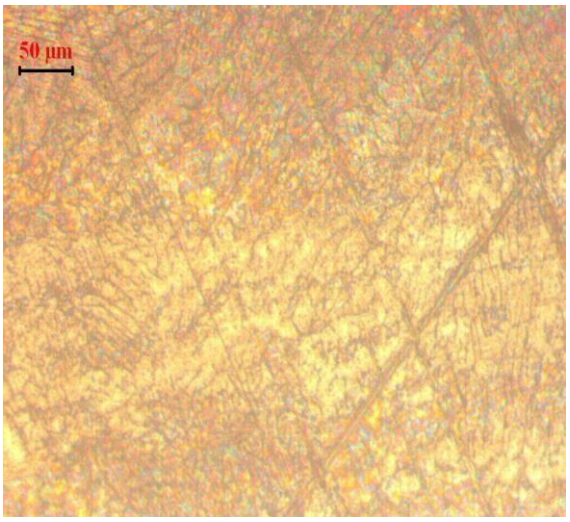

(b)

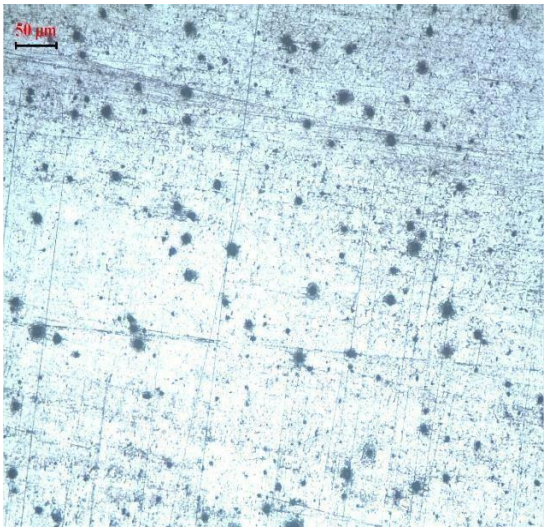

(c)

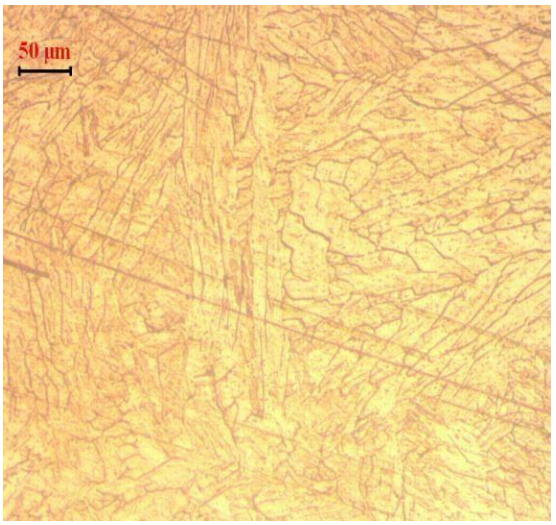

(d)

Figure 4.29: (a) Microstructural image for trial 7 (b) Microstructural image for trial 8 (c) Microstructural image for trial 9 (d) Microstructural image for trial 10

For the figure 4.29 (a), the various factors are short arc length, 220 amperes current, Filler ER308L, Full V groove and gas flow rate is 20 L/min. The figure is showing the worm like structure i.e. the vermicular structure. For the figure 4.29 (b), the various factors short arc, 200 Amps, ER 347, Double V groove and 23L/min. From the optical micrograph, a mixture of weld metal comprises of niobium contains microstructure when ferrite morphology has changed as compared to that of ER308L. From the figure 4.29 (c), the various factors are short arc, 220 Amps, fillers are ERNiCrMo-3, Half V and gas flow rate is 25L/min. This figure shows the retained ferrite in it. For the Figure 4.29 (d), the various factors are long

arc, current 140 Amps, ER 308 filler, Double V and 25 L/min. From the optical micrograph, weld metal comprises of ferrite dispersed in the austenitic matrix. The heat input variation encountered by this zone is clearly visible as some portion of the microstructure in the figure 4.29 (d).

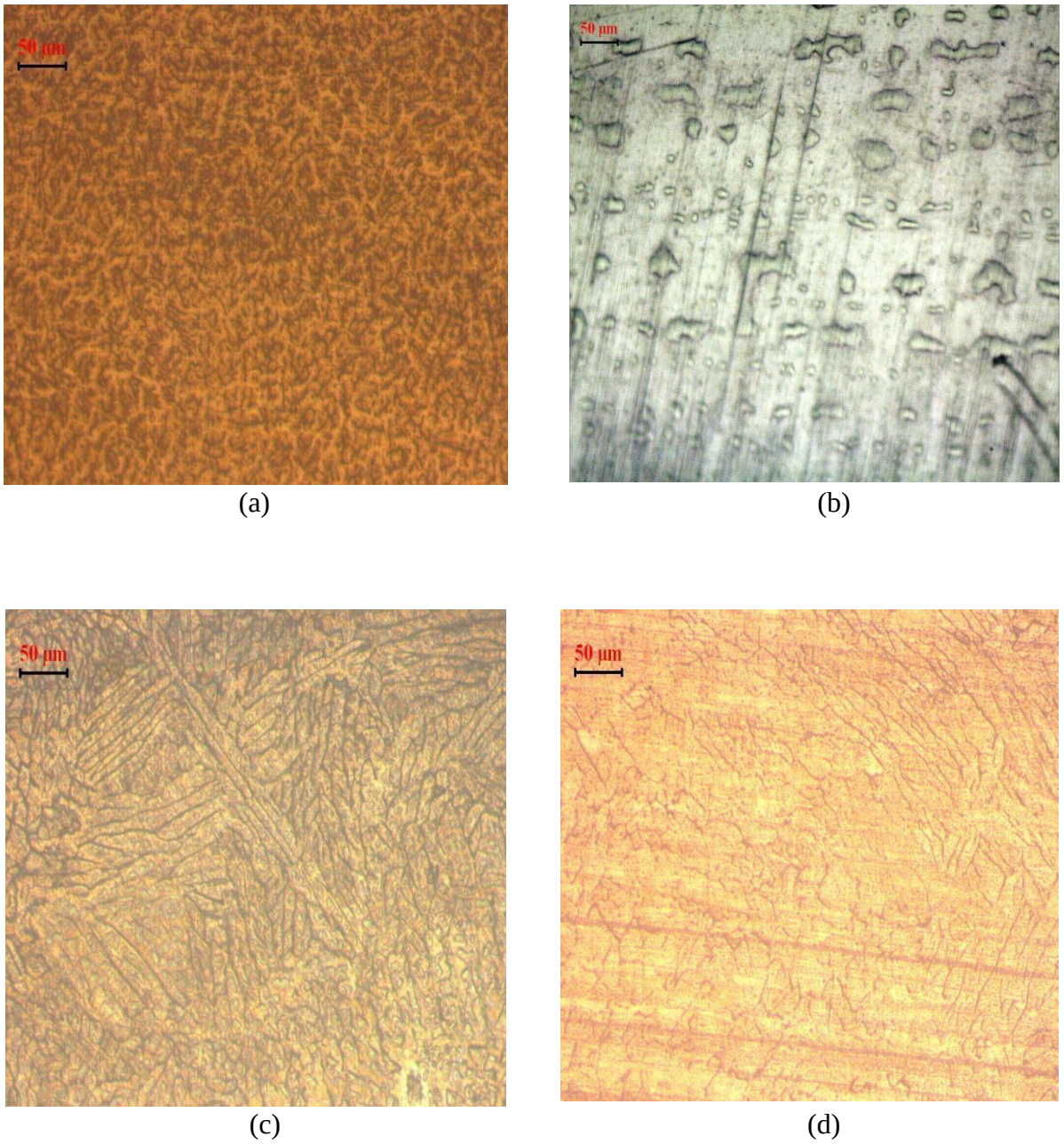

(a) (b)

(c) (d)

Figure 4.30: (a) Microstructural image for trial 11 (b) Microstructural image for trial 12 (c) Microstructural image for trial 13 (d) Microstructural image for trial 14

For the figure 4.30 (a), the factors taken are long arc, current 180 Amps, ER 347, Half V and gas flow rate is 20L/min. In this figure, the vermicular morphology is seen which is dispersed in austenitic matrix. For the figure 4.30 (b), the factors are taken long arc, 180 Amp current, filler ERNoCrMo-3, full V groove and 23 L/min gas flow rate, this figure shows directional solidification. For the Figure 4.30 (c), the various factors are taken long arc, current 200 Amps, ER 308L, Full V and 25 L/min. In this figure, the heat dissipation is executes such as an influence in which the inter-dendritic features of valuable nature are seen. For the figure 4.30 (d), the various factors taken are long arc, current 200 Amps, filler material is ER347, Double V groove and gas flow rate 20L/min. From the figure, it is analyzed that it has grain coarsening over there due to random solidification.

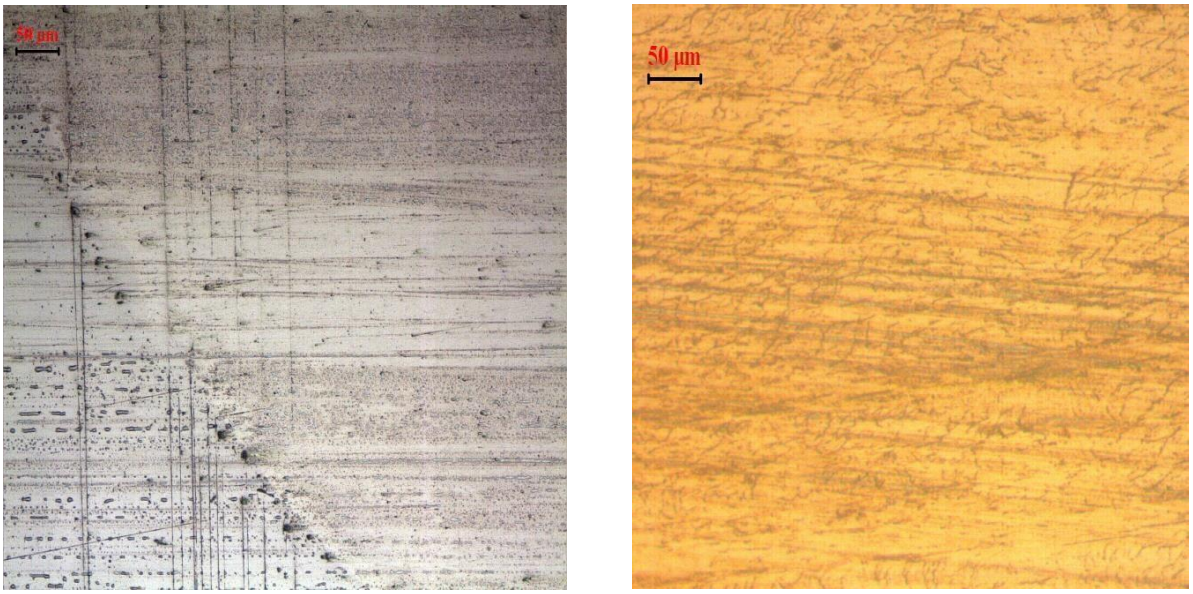

(a) (b)

Figure 4.31: (a) Microstructural image for trial 15 (b) Microstructural image for trial 16

For the figure 4.31 (a), long arc, current 200Amps, filler ERNoCrMo-3, half V groove and gas flow rate is 23L/ min. From the figure, inter-dendritic structures are analyzed. For the figure 4.31 (b), the various factors are long arc, Current 220 Amps, filler ER 308L, Double V groove and gas flow rate is 23L/min. In the figure, the skeleton morphology is seen and segregation of ferrite is also observed. From the figure 4.32 (a), the factors are long arc, current 220Amps, filler ERNiCrMo-3, Half V groove and gas flow rate 25 L/min. From the figure, it can be observed the coarse grain and some elongated grains with segregation. For the figure 4.32 (b), the process parameters are taken long arc, 220 Amps, ERNiCrMo-3, Full

V groove and 20 L/min. The micros structure is showing the inter- dendritic nature somewhat.

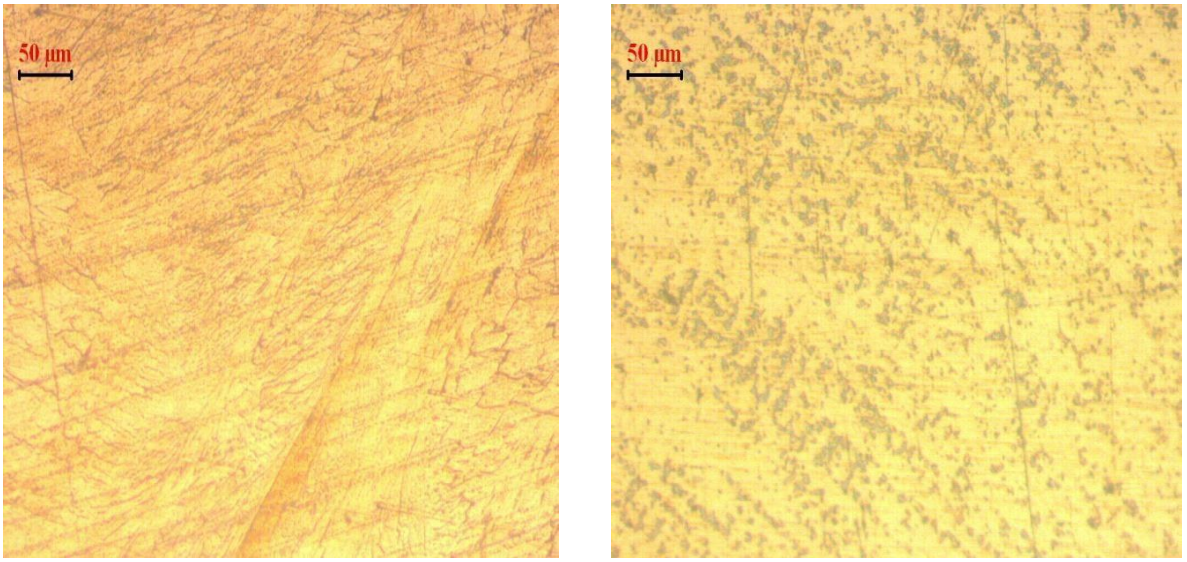

Figure 4.32: (a) Microstructural image for trial 17 (b) Microstructural image for trial 18

CHAPTER 5
CONCLUSION AND FUTURE SCOPE

5.1 CONCLUSION

The current analysis is done on the influence of the various parameter on the Gas Tungsten Arc Welding dissimilar weldments of SS316 and SS410. The different parameters are taken for welding operations i.e. arc length, current, type of fillers, type of grooves and gas flow rate. These parameters are optimize on different levels to get the optimize results. The conclusions of optimization are to be stated below

1) In the tensile test, the most significant factor are arc length and types of grooves. And the least effect is shown by the type of fillers. The maximum tensile strength is for 5^{th} trial (short arc length, current 200 Amps, Filler 347, Full V groove and gas flow rate is 25 L/min). The minimum tensile strength is for 11^{th} trial consisting the long arc, 180 Amps, filler 347, half V groove and gas flow rate is 20 L/min. From the SEM images it can be concluded that the fracture is ductile and most of the fracture arises at SS410 side.

2) The highest micro hardness is observed on the sample 3 which comprises the process parameters (short arc, current 220 Amps, ERNiCrMo-3, Double groove and gas flow rate 25 L/min) and minimum micro hardness is observed on the sample 8 with the process parameters (short arc, current 220 Amps, filler ER347, Double V and gas flow rate 23 L/min).The significant factor the current, arc length and type of filler. The least influential factor is gas flow rate.

3) The micro structures are showing a great variation from coarse grain structure to elongated grains. In this optical micrographs, the presence of δ-ferrite and austenite matrix is present.

5.2 Future Scope

1) Impact toughness test, SEM analysis of microstructures and radiography test are to be done.

2) Micro-structural and mechanical properties of dissimilar weld joints use by joining TIG, Laser and Laser-Tig welding.

3) Investigation on austenite stainless steel and nickel based super alloy dissimilar joints by TIG.

4) Corrosion behaviour of dissimilar weldments is to be done in aggressive atmosphere.

REFERENCES

[1] Mechanicalbuzz.com

[2] Kalpakjain and Schmid (2013), "Manufacturing engineering and technology" pearson publications

[3] Sindo kou (2003),"Welding metallurgy" a john willey and sos publications ISBN 0-471-43491-4.

[4] Wu, C. S., Gao, J. Q., Liu, X. F., & Zhao, Y. H. (2003). Vision-based measurement of weld pool geometry in constant-current gas tungsten arc welding. *Proceedings of the institution of mechanical engineers, Part B: Journal of Engineering Manufacture*, *217*(6), 879-882.

[5] http://www.bssa.org.uk/about_stainless_steel.php {accessed on 13/3/2017} [6] http://core.materials.ac.uk [acessed on 13/3/2017]

[7] Sureshkumar, L., Verma, S. M., Radhakrishna Prasad, P., Kiran Kumar, P., & Siva Shanker, T. (2011). Experimental investigation for welding aspects of AISI 304 & 316 by Taguchi technique for the process of TIG & MIG welding. *International Journal of Engineering Trends and Technology*, *2*(2).

[8] M. A. C. (2010). *Effect of Heat Treatment on the Corrosion Behavior of SS316 Stainless Steel in Simulated Body Environment* (Doctoral dissertation, UMP).

[9] Sakthivel, P., & Sivakumar, P. (2014). Effect of Vibration in Tig and Arc Welding Using AISI 316 Stainless Steel. *International Journal of Engineering, Research and Science & Technology*, *3*(4).

[10] Valsecchi, B., Previtali, B., Gariboldi, E., & Liu, A. (2011). Characterisation of the thermal damage in a martensitic steel substrate consequent to laser cladding process. *Procedia Engineering*, *10*, 2851-2856.

[11] www.threeplanes.net {acessed on 13/3/2017}

[12] Chander, G. S., Reddy, G. M., & Tagore, G. R. (2012). Influence of process parameters on impact toughness and hardness of dissimilar AISI 4140 and AISI 304 continuous drive friction welds. *The International Journal of Advanced Manufacturing Technology*, 1-13.

[13] S. V. Nadkarni (1988), “Modern arc welding technology”, Advani-Oerlikon limited.

[14] Arivazhagan, N., Singh, S., Prakash, S., & Reddy, G. M. (2011). Investigation on AISI 304 austenitic stainless steel to AISI 4140 low alloy steel dissimilar joints by gas tungsten arc, electron beam and friction welding. *Materials & Design*, *32*(5), 3036-3050.

[15] Falat, L., Svoboda, M., Výrostková, A., Petryshynets, I., & Sopko, M. (2012). Microstructure and creep characteristics of dissimilar T91/TP316H martensitic/austenitic welded joint with Ni-based weld metal. *Materials characterization*, *72*, 15-23.

[16] Chen, G., Zhang, Q., Liu, J., Wang, J., Yu, X., Hua, J., & Tang, W. (2013). Microstructures and mechanical properties of T92/Super304H dissimilar steel weld joints after high-temperature ageing. *Materials & Design*, *44*, 469-475.

[17] Hosseini, H. S., Shamanian, M., & Kermanpur, A. (2016). Microstructural and weldability analysis of Inconel617/AISI 310 stainless steel dissimilar welds. *International Journal of Pressure Vessels and Piping*, *144*, 18-24.

[18] Ramkumar, K. D., Dev, S., Saxena, V., Choudhary, A., Arivazhagan, N., & Narayanan, S. (2015). Effect of flux addition on the microstructure and tensile strength of dissimilar weldments involving Inconel 718 and AISI 416. *Materials & Design*, *87*, 663-674.

[19] Hajiannia, I., Shamanian, M., & Kasiri, M. (2013). Microstructure and mechanical properties of AISI 347 stainless steel/A335 low alloy steel dissimilar joint produced by gas tungsten arc welding. *Materials & design*, *50*, 566-573.

[20] Cao, J., Gong, Y., Zhu, K., Yang, Z. G., Luo, X. M., & Gu, F. M. (2011). Microstructure and mechanical properties of dissimilar materials joints between T92 martensitic and S304H austenitic steels. *Materials & Design*, *32*(5), 2763-2770.

[21] Ramkumar, K. D., Arivazhagan, N., & Narayanan, S. (2012). Effect of filler materials on the performance of gas tungsten arc welded AISI 304 and Monel 400. *Materials & Design*, *40*, 70-79.

[22] Ramkumar, K. D., Singh, A., Raghuvanshi, S., Bajpai, A., Solanki, T., Arivarasu, M. & Narayanan, S. (2015). Metallurgical and mechanical characterization of dissimilar welds of austenitic stainless steel and super-duplex stainless steel–A comparative study. *Journal of Manufacturing Processes*, *19*, 212-232.

[23] Kangazian, J., & Shamanian, M. (2017). Mechanical and microstructural evaluation of SAF 2507 and incoloy 825 dissimilar welds. *Journal of Manufacturing Processes*, *26*, 407-418

[24] Wang, J., Lu, M. X., Zhang, L., Chang, W., Xu, L. N., & Hu, L. H. (2012). Effect of welding process on the microstructure and properties of dissimilar weld joints between low alloy steel and duplex stainless steel. *International Journal of Minerals, Metallurgy, and Materials*, *19*(6), 518-524.

[25] Ramkumar, K. D., Anirudh, S., Singh, S., Goyal, S., Gupta, S. K., George, J. C., & Arivazhagan, N. (2017). Effect of fillers on the microstructure, mechanical properties, and hot corrosion behavior of Nb stabilized austenitic stainless steel welds. *Journal of Materials Research*, *32*(3), 582-598.

[26] Mukesh, S. S. (2013). Study of Mechanical Properties in Austenitic Stainless Steel Using Gas Tungsten Arc Welding (GTAW).

[27] Madhusudhan Reddy, G., Mohandas, T., Sambasiva Rao, A., & Satyanarayana, V. V. (2005). Influence of welding processes on microstructure and mechanical properties of dissimilar austenitic-ferritic stainless steel welds. *Materials and manufacturing Processes*, *20*(2), 147-173. [28]Qi, X., & Song, G. (2010). Interfacial structure of the joints between magnesium alloy and mild steel with nickel as interlayer by hybrid laser-TIG welding. *Materials & Design*, *31*(1),
605-609.

[29] Liu, L., Liu, X., & Liu, S. (2006). Microstructure of laser-TIG hybrid welds of dissimilar Mg alloy and Al alloy with Ce as interlayer. *Scripta materialia*, *55*(4), 383-386.

[30] Babu, N. K., Raman, S. G. S., Mythili, R., & Saroja, S. (2007). Correlation of microstructure with mechanical properties of TIG weldments of Ti–6Al–4V made with and without current pulsing. *Materials characterization*, *58*(7), 581-587.

[31] Choudhury, N., Bandyopadhyay, A., & Rudrapati, R. (2014). Design optimization of process parameters for TIG welding based on Taguchi method. *International Journal of Current Engineering and Technology*, 12-16.

[32] Kumar, A., & Sundarrajan, S. (2009). Optimization of pulsed TIG welding process parameters on mechanical properties of AA 5456 Aluminum alloy weldments. *Materials & Design*, *30*(4), 1288-1297.

[33] Lenin, N., Sivakumar, M., & Vigneshkumar, D. (2010). Process parameter optimization in ARC welding of dissimilar metals. *Thammasat International Journal of Science and Technology*, *15*(3), 1-7.

[34] Juang, S. C., & Tarng, Y. S. (2002). Process parameter selection for optimizing the weld pool geometry in the tungsten inert gas welding of stainless steel. *Journal of materials processing technology*, *122*(1), 33-37.

[35] Ross, P.J. (1995), "*Taguchi technique for quality engineering*," McGraw Hill publication".